Targeting different binding sites in the CFTR structures allows to synergistically potentiate channel activity

Lionel Froux, Ahmad Elbahnsi, Benjamin Boucherle, Arnaud Billet, Nesrine Baatallah, Brice Hoffmann, Julien Alliot, Renaud Zelli, Waël Zeinyeh, Romain Haudecoeur, et al.

Targeting different binding sites in the CFTR structures allows to synergistically potentiate channel activity

Lionel Froux[a,1], Ahmad Elbahnsi[b,1], Benjamin Boucherle[c,1], Arnaud Billet[a], Nesrine Baatallah[d,e], Brice Hoffmann[b,3], Julien Alliot[c,4], Renaud Zelli[c,5], Wael Zeinyeh[c,6], Romain Haudecoeur[c], Benoit Chevalier[d,e], Antoine Fortuné[c], Sandra Mirval[a], Christophe Simard[a,7], Pierre Lehn[f], Jean-Paul Mornon[b], Alexandre Hinzpeter[d,e,#], Frédéric Becq[a,2], Isabelle Callebaut[b,2*], Jean-Luc Décout[c,2]

a Laboratoire Signalisation et Transports Ioniques Membranaires, Université de Poitiers, 86073, France.

b Sorbonne Université, Muséum National d'Histoire Naturelle, UMR CNRS 7590, Institut de Minéralogie, de Physique des Matériaux et de Cosmochimie, IMPMC, 75005 Paris, France.

c Univ. Grenoble Alpes, CNRS, DPM, 38000 Grenoble, France

d INSERM, U1151, Institut Necker Enfants Malades, INEM, Paris, France

e Université de Paris, Paris, France

f INSERM UMR1078, IBSAM, Université de Bretagne Occidentale, Brest, France

1 These authors contribute equally

2 These authors contribute equally

** Corresponding author:* IMPMC, UMR7590 CNRS-Sorbonne Université, Case 115, 4 place Jussieu, 75252 Paris Cedex 05, France *; e-mail :* isabelle.callebaut@sorbonne-universite.fr

3 Present address : Iktos, Paris, France
4 Present address : Technologie Servier, Orléans, France
5 Present address : Institut de Recherches cliniques de Montréal, Montréal, Canada
6 Present address : ISPB-Faculté de Pharmacie, Université de Lyon 1, Lyon, France
7 Present address : Université de Caen, Caen, France

Summary declaration of interest: The authors declare the following competing financial interest related to their patent: Compounds for treating cystic fibrosis. I. Callebaut, J.-P. Mornon J.-L. Décout, F. Becq, Pierre Lehn, Brice Hoffmann, B. Boucherle, A. Fortuné, R. Haudecoeur, C. Boinot, WO 2016 087665 A2 20160609.

ABSTRACT

Recent evidence shows that combination of correctors and potentiators, such as the drug ivacaftor (VX-770), can significantly restore the functional expression of mutated Cystic Fibrosis Transmembrane conductance Regulator (CFTR), an anion channel which is mutated in cystic fibrosis (CF). The success of these combinatorial therapies highlights the necessity of identifying a broad panel of specific binding mode modulators, occupying several distinct binding sites at structural level. Here, we identified two small molecules, SBC040 and SBC219, which are two efficient cAMP-independent potentiators, acting at low concentration of forskolin with EC_{50} close to 1 µM and in a synergic way with the drug VX-770 on several CFTR mutants of classes II and III. Molecular dynamics simulations suggested potential SBC binding sites at the vicinity of ATP-binding sites, distinct from those currently proposed for VX-770, outlining SBC molecules as members of a new family of potentiators.

Keywords: CFTR, modulator, combinatorial therapies, 3D structure, Ussing chamber, halide-sensitive fluorescence

1. INTRODUCTION

Mutations in the Cystic Fibrosis Transmembrane conductance Regulator (*CFTR, ABCC7*) gene cause Cystic Fibrosis (CF), an autosomal recessive disease affecting approximately 80,000 people worldwide and characterized by progressive lung disease [1]. The CFTR protein is an epithelial anion channel, made of: (i) four well-folded domains (the Membrane-Spanning Domains MSD1 and MSD2, as well as the Nucleotide-Binding Domains NBD1 and NBD2), (ii) a regulatory (R) region showing intrinsic disorder and whose phosphorylation regulates channel activity, and finally (iii) N- and C-terminal segments, which mediate interaction with cellular partners [2]. More than 2,000 mutations have been reported so far, conferring a variety of molecular defects. The current classification of mutations into six different classes can be extended, by taking into account the observation of combinatorial defects for some of them and their susceptibility to modulators ([3]. Accordingly, the most common F508del mutation (a deletion of Phe508 in NBD1), impairs CFTR domain folding and folding cooperativity, leading to premature degradation (hallmark of class II mutations), but also leads to gating defect (as for class III mutations), as well as to instability at the plasma membrane (class VI mutations) [3]. Remarkably, it is now generally agreed that these defects can be rescued by combination of pharmacotherapies addressing single defects (i.e. correctors and potentiators acting respectively on protein maturation and channel function). Applying a corrector such as VX-809 (Lumacaftor) alone has little efficiency, while combining it to the potentiator VX-770 (Ivacaftor) improves function [4]. However, there is only modest clinical benefit [5] possibly due to remaining uncorrected single defects and increased turnover rate upon chronic VX-770 treatment [6, 7]. This therapeutic ceiling of first-generation correctors has led to the development of novel screening strategies for identifying second-generation correctors that could be used synergistically, in combination with the first ones [8]. Hence, it has recently been shown that combination of correctors exhibiting individually low rescue of F508del CFTR but acting through different mechanisms can robustly restore the functional expression of CFTR in human airway cells [9, 10]. Accordingly, one can distinguish: (i) type I correctors, targeting NBD1/MSD1 and NBD1/MSD2 interfaces, (ii) type II correctors, targeting NBD2 and/or its interfaces and (iii) type III correctors, acting on NBD1 folding/stability. This synergic action of correctors strongly suggests that several distinct binding sites are occupied within the CFTR protein. Occupation of these sites may moreover lead to a general rescue of mutated

proteins through allostery [10]. Along these lines, a triple combination of pharmacological chaperones (VX-809, RDR1 and MCG1516A) has also recently been reported, the three correctors having however been proposed to interact with NBD1 [11]. The importance of binding multiple sites for correction is now also underscored by the recent report of improved clinical efficiency when adding to ivacaftor (VX-770) + tezacaftor (VX-661) bitherapy new generation correctors (VX-445 and VX-659) targeting distinct sites of the protein [12, 13]. The search for alternative potentiators, which is following the same rationale of combinatorial therapy, remains required for mutations that appear refractory to treatment by single potentiators alone or for the use in combination with correctors, with no interference with the action of the latter or effect on protein stability [14-17].

The development of these combinatorial approaches highlights the importance of having a comprehensive inventory of the modulator binding sites within the CFTR protein 3D structure and identifying a broad panel of modulators. Potential binding sites, which may be targeted by drugs, have already been proposed (e.g. [18-24]), by considering models of 3D structures of the MSD:NBD assembly [25-27] and high-resolution cryo-EM 3D structures of full length CFTR in different closed conformations [24, 28-30]. Recently, a cryo-EM study has given a first view of a likely binding site for ivacaftor and GLPG1837, another CFTR potentiator, within the MSDs. However, the channel in the complex is still in a near open, closed conformation, although phosphorylated and ATP-bound [31].

In the present work, we have developed a series of small molecules (called SBC for *Small Binders of CFTR)*, initially designed for interacting with an obvious target site on CFTR, *i.e.* filling the pocket known to be present in the altered ICL4:NBD1 inter-domain interface in the F508del 3D structure. These molecules did however not display any obvious corrector activity, as expected from their design, but a potentiator activity was found in both F508del and wild-type CFTR, and variable effects were observed on several class III mutations sensitive to VX-770. A synergic effect was observed with VX-770 in comparison to SBC alone and VX-770 alone, suggesting that SBCs and VX-770 act through different sites and mechanisms. These features, associated with the SBC ATP-like purine scaffold, led to the hypothesis, supported by molecular dynamics (MD) simulations, that the SBC molecules act on the CFTR protein by occupying its ATP-binding site(s). This highlights the interest of such molecules as tools for a

pharmacotopological analysis of CFTR, allowing to better understand its mechanisms of action and opening new way for rational improvement of CFTR pharmacology.

2. RESULTS

2.1. Synthesis of a series of small CFTR binder compounds (SBCs)

We hypothesized that small molecules designed to occupy potential drug binding sites would lead to the discovery of new modulators of normal and defective CFTR chloride channel functions. A first series of small molecules was designed, by taking advantage of a model of the CFTR MSDs:NBDs assembly available at the beginning of this work [26], in which the molecules occupy the room left by the F508 deletion at the interface between NBD1 and ICL4 (F508del pocket, **Figure S1** (supporting information)). We chose to graft a phenyl group mimicking that of the F508 residue at the N9 of a purine bicycle scaffold, which is incorporated in many drugs and drugs candidates, for example, the cyclin-dependent protein kinase inhibitor (*R*)-Roscovitine (Seliciclib) [32]. The purine bicycle is made of five carbon and four nitrogen atoms well distributed in the bicyclic system. This distribution makes it a central scaffold in the search for pharmacological and therapeutic agents, being well adapted for H-bond formation, and the introduction of chemical functions and recognition elements at different positions on carbon and/or nitrogen atoms [33, 34]. In order to increase the solubility in water and to allow H-bonding from the phenyl ring, a carboxamido group $CONH_2$ was placed on the phenyl ring and, thus, the SBC001 structure appeared to be an interesting starting molecule allowing further chemical modifications by substitution of the C2 and C6 chlorine atoms. This structure was modified according to molecular docking in order to establish stronger interactions with the target sites and to preserve flexibility. Ten purines SBC001, 005, 040, 068, 069, 071, 183, 200, 219 and 231 carrying at position 9 a 4'-carboxamidophenyl group (**Fig. 1 and scheme 1 (A to I)**) were hence designed and, then, were chemically synthesized (Details of the synthesis are given in **Figure S2** (supporting information)). SBC001 was prepared by N^9-arylation of 2,6-dichloropurine in 16% yield through the Chan-Evans-Lam coupling reaction with (4-carbamoylphenyl)boronic acid and copper(II) [35]. Subsequent chloride substitution allowed the introduction of selected specific groups at position 6 and led to the 2-chloropurines SBC005 and SBC068. Preliminary chloride substitution from 2,6-dichloropurine afforded the 2-chloropurines SBC040 and 219 through N^9-arylation with (4-

carbamoylphenyl)boronic acid/copper(II) and with 4-iodobenzamide/copper(I) [36], respectively. These methods of N^9-arylation were used to prepare the 6-aminopurines SBC071 and 069, respectively, directly from 2,6-diaminopurine and *N,N*-(bis(*tert*-butoxycarbonyl)adenine. The synthesis of the purines SBC183, 200 and 231 was achieved from 5-amino-4,6-dichloropyrimidine and 2-amino-4,6-dichloro-5-formamidopyrimidine [37]. More recently, we developed a one-pot synthesis of highly functionalized purines from 4,6-dichloropyrimidines allowing for example the rapid and efficient preparation of SBC001 in 86% yield [38-40].

2.2. Characterization of the SBC activity

2.2.1. SBCs are not correctors of F508del-CFTR maturation

We first evaluated the effect of SBCs on F508del-CFTR maturation in Western-Blot experiments using stably transfected Hela cells expressing F508del-CFTR and an antibody directed against CFTR protein. The biochemical profiles of F508del-CFTR were similar in the absence or presence of any of the SBCs, tested as shown in **Figure S3** (supporting information). We used VX-809 as positive control to confirm the appearance of the mature form of CFTR (C band), an indicator of F508del-CFTR maturation correction. Thus, contrary to VX-809, SBCs are not correctors of F508del-CFTR maturation.

2.2.2. SBCs potentiate F508del- and wild-type (WT)-CFTR currents:

The ten purines synthesized were then screened for a possible potentiator activity using Ussing chamber experiments on CFBE F508del-CFTR cells corrected 24 h at 27°C to partially restore the membrane localization of the mutant. Compounds were sequentially tested at three concentrations: 10, 50 and 100 µM with a minimal pre-activation of CFTR with forskolin, an adenylate cyclase activator producing intracellular cAMP (0.1 µM; hereafter noted fsk) (**Fig. 2A and Fig. 2B**). We identified three compounds - namely, SBC001, SBC040 and SBC219 - able to elicit a significant $CFTR_{inh}172$-sensitive increase of the transepithelial short-circuit current (hereafter noted Isc) over fsk effect, others being inactive or producing very weak effects. Since SBC040 and SBC219 had the strongest effects, we considered them as leaders and determined their half-maximal effective concentration (EC_{50}) on CFBE F508del-CFTR cells (**Fig. 2C**). With fsk (0.1 µM) in the recording chamber, the EC_{50} values measured were 1.51 ± 0.21 µM (n= 4) for SBC040 and 0.87 ± 0.11 µM (n= 6) for SBC219. Consistent with data published

by other groups [41], EC_{50} value measured for VX-770 was almost 100 fold lower on these cells under our conditions (11.7 ± 1.5 nM; n= 6).

As the effects of SBC040 and SBC219 could be due to an augmentation of intracellular cAMP levels, we measured the intracellular cAMP concentration in CFBE F508del-CFTR cells after a 15-minute incubation with each SBC at concentrations leading to the maximal potentiator effect on F508del-CFTR (30 µM for SBC040 and 10 µM for SBC219). We did not detect any significant variation of intracellular cAMP levels after acute addition of the two leader compounds compared to solvent (**Fig. 2D**), suggesting their potentiator effect is not mediated by cAMP-PKA pathway activation.

Results obtained on CFBE F508del-CFTR were confirmed using automatic whole-cell planar patch-clamp on Hela cells stably expressing F508del-CFTR and corrected 24 h at 27°C (**Fig. 3**). We recorded a time and voltage independent current fully inhibited by 10 µM of $CFTR_{inh}172$ after the simultaneous addition of fsk (1 µM) + SBC040 (30 µM) or fsk + SBC219 (10 µM). The current densities recorded in the presence of SBC040 and SBC219 (at +40 mV: 38.2 ± 6.6 pA/pF (n=21) for SBC040 and 53.3 ± 9.6 pA/pF (n= 10) for SBC219) were significantly larger than the current density elicited by fsk alone (15.6 ± 1.9 pA/pF (n= 15) at +40mV), confirming the ability of SBCs to potentiate F508del-CFTR currents (p= 0.0011 for SBC040 and p= 0.0008 for SBC219; two-tailed Mann-Whitney test). Also, by comparison, the efficiency of SBC040 was similar to the clinically approved potentiator VX-770 effect (current density at +40 mV: 37.5 ± 5.7 pA/pF (n= 23) while SBC219 presented a stronger potentiation.

We also detected a potentiator effect on wild-type (WT)-CFTR in Hela cells with both SBCs, with a stronger effect of SBC219 (**Figure S4** (supporting information)). We did not observe major cytotoxic effects of SBCs as shown **Figure S5** (supporting information) in HeLa cells incubated for 24h with SBC040 or SBC219 at 1 and 10 µM. Of note is that the SBCs display activity at submaximal concentration of forskolin (0.1 µM) on F508del-CFTR, the effect disappearing at higher concentration (**Figure S6** (supporting information)). This behavior contrasts with the VX-770-mediated potentiation of CFTR, which is dependent on phosphorylation level [42] (see below and discussion). Several CFTR potentiators are known to interfere with the correction of F508del-CFTR maturation defect by VX-809 or VX-661 [6,

7]. Preliminary data obtained by western-blot suggest that SBC040 have a negative effect on VX-809 correction, in the same range as VX-770 (data not shown).

2.2.3. Effect of SBC040 and SBC219 on G551D and G1349D mutations, and class III mutations

Then, we tested the potentiator effect of the two SBC leaders on two major class III CFTR mutants: G551D and G1349D, which are sensitive to VX-770 [43], the potentiator used to treat the resulting cystic fibrosis. These two amino acids occupy similar positions in the ABC signature of NBD1 and NBD2, respectively, bordering the canonical and non-canonical ATP-binding sites, respectively. The SBC effect was first evaluated using conventional whole cell patch-clamp on Hela cells transiently transfected with a pEGFP-CFTR-G551D or -G1349D (**Fig. 4**). While no potentiation of CFTR Cl^- currents was observed with SBC040 on both mutants (**Fig. 4** *top panels*), application of 10 µM SBC219 elicited a 2.6 fold potentiation of fsk pre-activated CFTR current (**Fig. 4** *bottom panels*) for both mutants. These Cl^- currents recorded were fully inhibited by the $CFTR_{inh}172$. However, the potentiation of CFTR current by SBC219 was not maximal on these mutants since the current elicited when using SBC219 remained lower than when the investigational CFTR potentiator genistein was used.

We evaluated the effect of SBCs on class III CFTR mutants expressed in HEK293 cells using a halide sensitive YFP assay. In control WT-CFTR expressing cells, SBC040 and SBC219 potentiated CFTR activity at both 10 µM and 50 µM to a slightly lower level to that observed with VX-770 (**Fig. 5A**). G551D and G1349D were found to be responsive to VX-770 treatment, with higher correction achieved for G1349D as compared to G551D. A stronger effect was observed for SBC219 on G1349D compared to SBC040 (**Fig. 5A**). Interestingly, the effect of both SBC040 and SBC219 were more pronounced on G551S CFTR (**Fig. 5A**), suggesting an effect of the length or polarity of the side chain introduced in the canonical binding site. The sensitivity to SBC040 and SBC219 of two additional class III mutations, sensitive to VX-770 and located within NBD2, was also tested. The first one (G1244E) is located within the canonical ATP-binding site, in front of NBD1 G551D. This mutation showed similar low responses regarding the effect of SBC040 and SBC219 (**Fig. 5A**). In contrast, S1255P, which is located farther from the canonical binding site, displays responses to both SBC040 and SBC219 (**Fig. 5A**). Finally, the sensitivity to SBC040 and SBC219 of a VX-770-sensitive class III mutation located in ICL3 (G970R) was also tested. This mutation showed increased levels of responses

with SBC040 and SBC219, with a level of potentiation reached by SBC219 at 50 µM similar to that of VX-770 at 10 µM (**Fig. 5A**).

2.2.4. Potentiator effect of SBCs is synergic with VX-770 effect and compatible with VX-809 correction

We then addressed the question of a potential interaction with correctors or other potentiators. We therefore compared the effects of SBC040 and SBC219 to the effect of VX-770 on CFBE F508del-CFTR cells treated 24 h with VX-809 before Ussing chambers experiments. We also added VX-809 (10 µM) to the apical solution 5 min before protocol starting to ensure the presence of the molecule during the whole experiment. During these experiments, SBCs were added either before or after VX-770 and were used at concentrations leading to their maximal effect. We also added fsk (0.1 µM) to pre-activate CFTR before SBC or VX-770 addition (**Fig. 6A**). When focusing on the effect of each compound added alone, the variation of Isc (noted ΔIsc and defined as the variation of I_{sc} induced by the addition of a compound to the apical membrane) was significantly lower after SBC addition (1.2 ± 0.2 µA.cm^{-2} for 040 and 0.91 ± 0.11 µA.cm^{-2} for 219, n= 7) than after VX-770 addition (3.0 ± 0.2 µA.cm^{-2}, n= 14). However, when adding SBC and VX-770 sequentially, ΔIsc increased when compared to VX-770 alone (5.1 ± 0.3 µA.cm^{-2} with 040 or 6.3 ± 0.5 µA.cm^{-2} with 219 vs. 3.0 ± 0.2 µA.cm^{-2} alone, n=14) (**Fig. 6B**) suggesting an additivity or a synergy between SBC and VX-770 effects. Of note is that the combination of SBCs and VX-770 at low forskolin concentration leads to effects greater than those obtained for VX-770 alone at high forskolin concentration (**Figure S6** (supporting information)). This effect, even at lower phosphorylation level of CFTR, demonstrates the interest of SBCs despite the absence of effect alone at high forskolin concentration.

We then focused the data analysis on the repartition of the different effects, depending on the order in which the compounds were added (**Fig. 6C and Fig. 6F**). As expected, we noticed a significant effect of the compounds ($p< 0.0001$ for both SBCs; n= 7) but not of the order in which the compounds were added on ΔIsc ($p= 0.45$ for SBC040 and $p= 0.88$ for SBC219; n=7). The statistical analysis also returned a positive result for interaction significance, suggesting the order in which the compounds were added could have influenced their individual effects. This hypothesis is supported by the fact that there is a significant difference between VX-770

and SBC effects when SBCs were added before VX-770 but not when SBCs were added after VX-770 (for both SBCs: $p< 0.001$; n= 7). This suggests a possible synergy between SBCs and VX-770 effects besides additivity. To confirm this, we used the same data set and focused our attention on the amplitude of the VX-770 effect, whether VX-770 was added alone or after SBC040 or SBC219. The same comparison was done between the effect of SBC040 or SBC219 alone or after the addition of VX-770. We noticed a significant augmentation of VX-770-induced ΔIsc when SBC040 (**Fig. 6D**; 2.82 ± 0.22 $\mu A.cm^{-2}$ vs 3.84 ± 0.26 $\mu A.cm^{-2}$; n= 6-7; p= 0.035) or SBC219 (**Fig. 6G;** 3.12 ± 0.34 $\mu A.cm^{-2}$ vs 5.45 ± 0.59 $\mu A.cm^{-2}$; n=7; p=0.002) was added before VX-770 and of SBC-induced ΔIsc when VX-770 was added before SBC040 (**Fig. 6E;** 1.21 ± 0.20 $\mu A.cm^{-2}$ vs 2.57 ± 0.44 $\mu A.cm^{-2}$; n= 7; p= 0.007) or SBC219 (**Fig. 6H;** 0.91 ± 0.11 $\mu A.cm^{-2}$ vs 3.02 ± 0.48 $\mu A.cm^{-2}$; n= 7; p= 0.0006), even if this effect was larger for SBC- than for VX-770-induced ΔIsc. Taken together, these results show that SBCs are able to potentiate F508del-CFTR current in the presence of VX-809 and that the effects of SBCs and VX-770 are synergic.

The synergy of SBCs with VX-770 was also evaluated using the YFP halide sensitive assay. No further potentiation was observed for WT-CFTR, using either SBC combination or VX-770 with either SBC (**Fig. 5B**). This was in contrast to results obtained with G551D-, G970R- and G1349D-CFTR (**Fig. 5B**). Both SBCs indeed showed stronger effect with VX-770 on these three mutated proteins, enabling to restore WT levels of CFTR function. Moreover, these results suggest a synergy between SBC and VX-770 effects on G551D-, G970R- and G1349D-CFTR since the effect of SBC040 or SBC219 combination with VX-770 was greater than the sum of SBCs and VX-770 individual effects on these mutants.

2.3. Mapping SBC potential binding site(s)

As the two SBC040 and SBC219 act in a synergistic way with VX-770, we hypothesized that they may bind site(s) distinct from this/those occupied by VX-770, for which several evidences now indicate potential binding sites within the MSDs (see Discussion). As the SBCs act on WT-CFTR, we also ruled out a potential binding site at the interface between ICL4 and NBD1 (F508del pocket), as initially targeted on the model of F508del-CFTR 3D structure. Given the SBC general scaffold and the fact that SBC040 has no or poor potentiation effect on the G551D and G1349D-CFTR contrary to WT-CFTR (see above), a consistent hypothesis for the SBC-binding sites (at least SBC040) should be within one or both ATP-binding sites. To test this

hypothesis, we first docked SBC040 and SBC219 in the two free ATP-binding sites within the model of the 3D structure of the wild-type CFTR MSDs:NBDs assembly in an open conformation, as previously published [25]. We used this model rather than the more recent cryo-EM 3D structures of phosphorylated, ATP-bound zebrafish and human CFTR [29, 30], as these last ones are yet in a closed conformation, even when solved in complex with ivacaftor, as recently reported [31]. The reliability of the whole models has however been supported by comparison with these experimental 3D structures [44]. The conformations of the NBD1:NDB2 assembly and of their interfaces with the ICLs are moreover highly similar, as illustrated in **Figure S7** (supporting information)**.**

The results of this docking on the CFTR 3D structure model were supported by an automatic docking performed using the Autodock Vina and AutoDockTools (45 % of the 20 best hits in a docking experiment performed on NBDs felt within the ATP-binding sites). Molecular Dynamics (MD) simulations on SBC040 and SBC219 docked within the canonical and non-canonical ATP-binding sites were then performed over periods > 100 ns for testing their adaptation to/stability in these sites and identifying of critical residues. Overall stability of the trajectories is observed from 50-60 ns, as appreciated by stable RMSD values, not only for the wild-type constructs, but also for F508del (simulation performed at 300 K) (**Figure S8** (supporting information)). Notably, in the bound complexes, the CFTR MSDs:NBDs assembly displays features of the open conformation, as illustrated for instance with the presence of salt bridges between E267 (ICL2) and R1060 (ICL4) [45, 46] and between R352 (TM6) and D993 (TM9) [47, 48] (data not shown). During simulations, the SBC molecules stayed at the level of ATP-binding sites, but their positions differently evolved according to the considered ligand and ATP-binding site, with significant plasticity observed to accommodate the ligand to the binding site. Maps of contacts between SBC and CFTR amino acids were established along simulations, allowing to accurately define amino acids participating in binding and identify the most representative conformations by cluster analysis (See Material and Methods, **Figure S9** (supporting information)). SBC features in the canonical and non-canonical binding sites of WT-CFTR (most populated clusters) are detailed in **Fig. 7** and **Figure S10** (supporting information). In the canonical binding site, SBC040 occupies the ATP binding site, with contacts limited to NBD1 and NBD2 residues. In NBD1 are involved amino acids of the ABC signature (of which Q552 which makes a hydrogen bond with the SBC040 O amide) and other

amino acids of the α-subdomain (of which F533, L541 and T547). In NBD2, are principally involved amino acids of the Walker A motif, of which the G1247 N main atom making an H-bond with the SBC040 N amide. In contrast, SBC219 occupied an upper position, with several contacts with amino acids from ICL2 (of which Q270) and ICL3 (including M961 and N965). Of note is the NBD2 A loop Y1219 (which stacks the ATP adenine ring) makes critical contacts with the purine ring of both SBC040 and SBC219 in the canonical ATP-binding site. In addition, in SBC219, two N atoms of the purine ring make H bonds with the Y1219 main chain oxygen atom. Notably, there was significant reorganization of the residues within the ATP-binding site to accommodate ligands, as assessed by calculation of backbone "cross" RMSD on the conserved motif of the ATP-binding sites (**Figure S11** (supporting information)). Interestingly, the position of SBC040 and SBC219 at the level of the ATP-binding site after MD simulation are similar in the wild-type protein and in the F508del construct, involving similar contacts (**Figure S12** (supporting information)). The same situation is observed between wild-type CFTR and G551D CFTR (**Figure S13** (supporting information)). At the level of the non-canonical ATP-binding site (**Fig. 7**), which is covered by the large regulatory insertion (RI), SBC040 and SBC219 principally make contacts with NBD1 (and very few with NBD2). As at the level of the canonical binding site, the A loop aromatic side chain (W401) is also involved in SBC binding. However, the two SBC molecules are positioned differently, SBC219 being located in an upper position, in the vicinity of the NBDs:ICLs interface. Again, there was significant reorganization of the residues within the ATP-binding site to accommodate ligands, as assessed by calculation of backbone cross RMSD on the conserved motif of the ATP-binding sites (data not shown).

Based on the performed simulations, free energy binding values were estimated according to Molecular Mechanics/Generalized Born Surface Area (MMGBSA) calculations. Values obtained for SBC219 in both the canonical (-35.4 ± 4.5 kcal/mol) and non canonical (-35.3 ± 4.1 kcal/mol) are similar and greater than those obtained for SBC040 (-15.3 ± 4.9 and -21.3 ± 3.2 kcal/mol, respectively). Considering these values thus does not allow to favor one site over another for SBC binding.

3. DISCUSSION

In light of the current efforts developed today towards combinatorial pharmacotherapy, mapping in a comprehensive way the different possible binding sites of modulators which may

act in an additive or synergic way, is of outmost importance. However, except from a possible binding site for ivacaftor recently highlighted within the MSDs using cryoelectron microscopy [31], no direct experimental evidence describing CFTR modulator-binding sites is available, which can be considered to explain the molecular mechanisms involved in the modulation and to provide insights for improving existing molecules or designing new ones.

Several observations have however led to suggest different potential sites for correctors and potentiators. The lack of two secondary structure elements (strand s5 and helix h2) in CFTR NBD1 relative to standard ABC NBDs leads to an imperfect ball-and-socket joint at the interface between NBD1 and MSDs (more exactly in the space separating intracellular loops ICL1 (from MSD1) and ICL4 (from MSD2)), offering a potential binding site that could be targeted by drugs [19, 24]. Another potential binding site is provided at the interface between ICL4 and NBD1, when F508 is absent (F508del pocket). This site has logically been explored as a potential corrector-binding site [20] and overlaps the putative binding site of some correctors identified by virtual screening using the F508del NBD1 3D structure [22]. This F508del pocket was also targeted for the design of the SBCs discussed herein, but it has however been discarded as their actual binding site, due to the potentiation activity of the compounds also observed on the wild-type CFTR protein. *In vitro* studies have provided information about the mechanism of action of VX-809, which stabilizes MSD1, involving amino acids Phe374 and Leu375, in the early steps of co-translational folding [49, 50]. Based on this information, a potential VX-809-binding site has been identified by molecular docking at the bottom of MSD1, including Phe374 and Leu375 at the end of TM6 ([21] and our unpublished results). Two studies have also proposed that Lumacaftor can bind NBD1 [11, 51]. Finally, putative binding sites of type III correctors (acting on NBD1 folding/stability) can be searched at the surface of (or buried within) NBD1. These investigations are encouraged by the effects of stabilizing mutations [52] or stabilizing nanobodies [53], but so far, NBD1 binders have however shown either (i) low affinity (*e.g.* CFFT-01 and BIA (bromoindole-3-acetic acid), which both bind to an inner NBD1 pocket) [54]) or (ii) no activity on full length F508del CFTR [16], precluding their development as correctors [55]. Higher affinity type III correctors have very recently been proposed (4172 compound in [10]), but their NBD1 binding sites remain to be unveiled; it is also the case for the c407 molecule which has been previously proposed as NBD1-specific [22]. The difficulty in addressing putative corrector binding sites is amplified by

the fact that some of these molecules may bind conformations transiently occurring in the early steps of co-translational folding, but no longer existing in the final native protein like conformation. Of note is that the small size of the SBC molecules and the flexibility of SBC219 in comparison to the size and rigidity of correctors VX-809, -661, -445 and -659 are probably disadvantages to induce an efficient folding and long-term stability of F508del CFTR. In the search for correctors from the purine scaffold, SBC001 could be used to introduce large and rigid chemical groups through substitution of the 6-chlorine atom.

In the field of potentiators, mechanistic studies have proposed that these compounds may act on the energetic coupling between NBD dimerization and gate opening /closing in the MSDs [56], shifting gating transitions to favor the open state. This may be performed (i) at the level of the NBD dimer, by acting on the interface between the NBD1 and NBD2, as targeted by ATP analogues (N^6-(2-phenyl-ethyl)-ATP (PATP) [57-59], 2'-deoxy-ATP (dATP) [60, 61] and 2'-deoxy-N^6-(2-phenyl-ethyl)-adenosine-5'-*O*-triphosphate (dPATP [62])) or (ii) at the level of the MSDs, at the interface between the lipid core of the membrane, as proposed for VX-770 and a more recent potentiator, GLPG1837 [63-66]. Hydrogen/deuterium exchange studies have indicated some regions particularly affected by VX-770 binding, at the interface between MSD2 and NBD1 and between MSD2:NBD2 [18], thus distinct from the ATP-binding and MSD-binding sites. More recently, ivacaftor/ GLPG1837 binding site(s) have been mapped by docking the compounds on the 3D structures of the CFTR protein [23] and within an EM density likely corresponding to the drugs within the protein-drug complex [31]. The mechanisms of action and binding site(s) of a third group of potentiators (5-nitro-2-(3-phenylpropylamino)benzoate (NPPB)) [67, 68] remain unsettled, as well as those of novel co-potentiators (arylsulfonamide-pyrrolopyridine ASP11), which activate wild-type CFTR in the absence of a cAMP agonist [16].

Here, we have identified potentiator effects induced by a series of yet un-optimized molecules, which act both, as VX-770, on F508del and wild-type CFTR. The effect of SBCs on F508del-CFTR does not seem to depend on the type of correction used since it was observed on both temperature- (screening assays and patch-clamp) and VX-809- (Ussing chamber) corrected cells and was not affected by the presence of VX-809 during Ussing chamber experiments. We also show that SBCs act in a synergic manner with VX-770 on several CFTR

mutants (F508del, G551D, G970R and G1349D). There are now several studies emphasizing the interest of co-potentiators which act in an additive way or allosterically [8, 16, 17, 69-71], some of them being particularly interesting relative to their lack of interference with corrector activity [8, 17], their nanomolar potency and their effect on VX-770 insensitive mutations, such as N1303K and W1282X [16, 70]. SBCs remain to be optimized and their effects to be tested compared to other potentiators (for instance Asp11) and against a large panel of CFTR pathogenic mutations, especially those which are not addressed by the recently described class II potentiators, essentially active on mutations in CFTR NBD2 [70]. Even though we observed a negative effect of SBC040 on VX-809 correction of F508del CFTR, as it is the case for VX-770 and other potentiators [6, 7], SBCs may be of particular interest for their activity at submaximal concentration of forskolin, as observed for ASP-11 [16], contrasting with the dependence of VX-770 on the CFTR phosphorylation state [42]. According to Cui and colleagues [42], such drugs acting on sub-maximally activated CFTR are likely more physiologically relevant than those screened against CFTR channels activated by high concentrations of PKA activators. Further developing such drugs may enable the discovery of more potentiators, active on VX-770-resistant mutations, by increasing the dynamic range and avoiding ceiling effects.

On another hand, SBCs can be considered as tools to understand the mechanisms at play in CFTR (co-potentiation), in particular relative to our theoretical data, which suggested potential binding sites at the level of ATP-binding sites, with a noticeable evolution of the protein conformation to adapt such small molecules and possibly to allow allosteric regulation of the CFTR channel activity. The relevance of such potentiator binding sites at the NBDs interface has already been supported by other docking experiments based on 3D models [72, 73], but remains to be supported at the experimental level. Of note, the free energy binding values calculated here are lower for SBC219 than for SBC040 in the two potential binding sites, a result consistent with (i) the higher efficiency observed for SBC219 and (ii) with the additional contacts predicted to exist between SBC219 and the intracellular loops (at least at the level of the canonical ATP-binding site). SBC219 is particularly interesting as it is positioned, at the level of both sites, in between the ATP-binding sites and ICLs. Based on this theoretical work and its inherent limitations, it is not possible to favor one site over the other, but the clear differences observed between the binding sites open perspectives for further

characterization and optimization. The canonical binding site seems particularly appealing as the two NBDs are involved in SBCs binding, thereby enabling the stabilization of the tight interdomain interface, hallmark of the CFTR open conformation. Moreover, it also includes, in the specific case of SBC219, amino acid residues from the intracellular loops (ICLs), thus possibly amplifying allosteric communication with the MSDs and subsequent channel opening. Maintaining an ATP-bound-like conformation at the canonical ATP-binding site might prevent closure of the CFTR channel [74]. It is interesting to note that according to our MD simulations, SBC040 might however still be able to bind in the vicinity of the canonical ATP-binding site in the G551D-CFTR protein, as the aspartic acid residue has no direct contact with SBC040 (in contrast to the situation where ATP is bound in the ATP-binding site [73]), whereas the drug has low or no potentiator effect when used alone on the mutated protein. This absence of effect may be due to additional bonds that the aspartic acid might form within the site, which lower the flexibility necessary for allosteric channel opening at the level of MSDs.

The synergy observed here between VX-770 and SBCs and the theoretical data gained by MD simulations suggest that obtaining an optimal gating signal might involve distinct sites present (i) at the level of the NBDs (allowing their optimal association and interaction with the ICLs) and (ii) at the level of the MSDs (allowing to shift the equilibrium towards an open conformation of the channel). This synergic (and not only additive) behavior, which was not observed for other recently developed potentiators ([14-17], might suggest that binding of one ~~drug~~ molecule to one site may allow allosteric switching towards an intermediate active conformation, which is then prone to elicit an optimal response to the second drug. Further studies, involving especially MD simulations with drugs bound in their respective binding sites, are required to further decipher the molecular mechanisms of allosteric potentiation, which in turn may inform drug design efforts.

4. Experimental section

4.1 SBC synthesis and characterization

All starting materials were commercially available research-grade chemicals and used without further purification. Reactions were monitored by analytical TLC on silica gel (Alugram Sil G/UV_{254}) from Macherey–Nagel with fluorescent indicator UV_{254}. ^{1}H NMR spectra were

recorded on a Bruker Avance 400 at 400 MHz. ^{13}C NMR spectra were recorded either on a Bruker Avance 400 or on a Bruker Avance 500, respectively at 100 or 126 MHz. Chemical shifts are reported in ppm (parts per million) relative to the residual signal of the solvent in which the spectrum was recorded [^{1}H: δ(*d*$_6$-DMSO) = 2.50 ppm, δ($CDCl_3$) = 7.27 ppm, δ(CD_3OD) = 3.31 ppm; ^{13}C: δ(*d*$_6$-DMSO) = 39.52 ppm, δ($CDCl_3$) = 77.16 ppm, δ(CD_3OD) = 49.00 ppm], and the signals are described as singlet (s), broad singlet (bs), doublet (d), triplet (t), multiplet (m). Coupling constants are reported in Hertz (Hz). Column chromatography purifications were performed on a Grace Reveleris X1 apparatus, using Grace Resolv silica gel cartridges (40 µm). HRMS analyses were obtained from the Mass Service, ICOA, at the University of Orléans, France, using a HRMS Q-Tof MaXis spectrometer. Combustion analyses were obtained from the analysis facilities of DCM, Grenoble, France. HPLC analyses were performed with an Agilent 1100 series using a diode array detector and a C_{18} reversed-phase column (Nucleodur C_{18} ISIS, Macherey–Nagel, 5 µm particle size, 250 mm × 4.6 mm), with a mobile phase composed of A= H_2O and TFA 0.1% and B= MeOH and TFA 0.1% with a gradient 100:0 to 0:100 A:B over 20 min, 1 mL/min, 10 µL injection, detection at 254 nm.

Purity of the reported compounds was determined by combustion analysis or HPLC analysis and in every case appeared to be ≥ 95%. Details of the different syntheses are given in **Fig. S2** (supporting information).

4.2. SBC activity

4.2.1. Cell culture

All cell lines were grown at 37°C in 5% CO_2 - 95% air and media were replaced every 2 days. Human bronchial epithelial cell lines were provided by Dr. D. Gruenert (Univ. California San Francisco, USA). CFBE41o$^-$ cells overexpressing F508del-CFTR (CFBE F508del-CFTR) were grown on TPP culture flasks in Eagle's Minimum Essential Medium (EMEM) containing non-essential amino acids (NEAA) (Gibco 10370) supplemented with 10% fetal bovine serum (FBS) (Sigma), 2 mM L-glutamine (Gibco), 50 IU.mL^{-1} penicillin (Sigma), 50 µg.mL^{-1} of streptomycin (Sigma) and were selected using 5 µg.mL^{-1} puromycin (Gibco). HeLa and HeLa F508del-CFTR cell lines were grown on TPP culture flasks in Dulbecco's Modified Eagle's medium containing glutamine and pyruvate (Gibco 31966) supplemented with 9% FBS (Sigma), 50 IU.mL^{-1} penicillin and 50 µg.mL^{-1} streptomycin. Zeocin (50 µg.mL^{-1}, Invitrogen) was used as selection antibiotic for Hela F508del-CFTR cell line. Hela cells were transiently transfected with either

pEGFP G551D-CFTR or pEGFP G1349D-CFTR cDNA constructs (0.5 µg.mL^{-1}) using cationic lipids (JetPEI, QBiogene) to express G551D-CFTR or G1349D-CFTR respectively. Cells were used 48h post-transfection. To study the potentiator effect of our compounds on F508del-CFTR, sufficient levels of the protein were restored to the plasma membrane by incubating cells at 27°C or with 10 µM VX-809 during 24 h prior experiments.

HEK293 cells purchased from ATCC were cultivated on Falcon culture flasks in Dulbecco's Modified Eagle's medium containing GlutaMax (Gibco 61965) supplemented with 10% FBS (Gibco). HEK293 cells were transiently co-transfected with both halide-sensitive YFP-H148Q/I152L and pTracer WT-CFTR or mutant CFTR cDNA constructs using cationic lipids (Turbofect, Fermentas). Mutagenesis was performed using the QuickChange XL II mutagenesis kit (Agilent) following the manufacturer's instructions using the cDNA of CFTR (M470). Obtained mutants were fully sequenced, amplified, purified (Macherey-Nagel) and plasmid concentrations measured using a Nanodrop (Thermo Fisher Scientific). After 24h, cells were transferred to poly-L-lysine coated 96 well black/clear bottom microplates 96 well plate.

4.2.2. Whole-cell patch-clamp recordings

For manual patch clamp, Cl^- currents were measured in the whole-cell patch-clamp configuration using an Axopatch 200B amplifier connected to an analog/digital interface, Digidata 1440A, and were analyzed using pCLAMP 9 software (all from Axon Instruments Inc., Burlingame, CA, USA). The holding potential was -40 mV and voltage pulses from -100 to +100 mV in 20 mV increments were applied to record CFTR currents. Pipettes were pulled from borosilicate glass capillaries (GC150-TF10; Clark Electromedical Inc., Reading, UK) and connected to the head stage of the patch clamp amplifier through an Ag–AgCl wire (pipette resistance 3-4MΩ). Pipette capacitance was electronically compensated in cell-attached mode. The external bath solution contained (in mM): 145 NaCl, 4 CsCl, 1 $CaCl_2$, 1 $MgCl_2$, 10 glucose, and 10 TES (titrated with NaOH to pH 7.4). The osmolarity was 315 ± 5 mOsmol. The intrapipette solution contained (in mM): 113 L-aspartic acid, 113 CsOH, 27 CsCl, 1 NaCl, 1 $MgCl_2$, 1 EGTA, 1 TES, and 3 Mg-ATP (titrated with CsOH to pH 7.2). The osmolarity was 285 ± 5 mOsmol.

Automated whole-cell patch clamp (APC) recordings were performed and analyzed as described previously [75]. Briefly, experiments were performed on the eight-channel Patchliner NPC-16 workstation (Nanion Technologies GmbH, Munich, Germany), which was coupled to two QuadroEPC-10 amplifiers (HEKA Elektronik GmbH, Germany). APC procedures

followed Nanion's standard procedures and used Nanion's high-resistance chips. The holding potential was maintained at −40 mV throughout the experiment. To record CFTR currents, pulses from the holding potential of −40 mV to test potentials between −80 and +80 mV in 20 mV increments were used. External solution contained (in mM): 145 NMDG, 145 HCl, 10 TES, 5 $BaCl_2$, 2 $CaCl_2$, 2 $MgCl_2$ (titrated with NMDG to pH 7.4). The osmolarity was 300 ± 10 mOsmol. Internal solution contained (in mM): 105 NMDG, 30 H_2SO_4, 20 HCl, 10 TES, 10 EGTA, 4 $MgCl_2$, 3 Mg-ATP (titrated with HCl to pH 7.2). The osmolarity was 285 ± 5 mOsmol. All patch clamp experiments (manual and automatic) were conducted at room temperature (20 –25 °C).

4.2.3. Short-circuit current measurements

CFBE CFTR-F508del cells were seeded at a density of $0.5x10^6$ cells on Snapwell permeable inserts (#3407, Corning Corp.) coated with human fibronectin (5 $\mu g.cm^{-2}$; Sigma). After 2 days at liquid/liquid interface, cells were cultured at air/liquid interface until transepithelial resistance reached a minimum of 300 $\Omega.cm^{-2}$ (5-6 days). Transepithelial resistances were measured with a Millicell-ERS voltmeter-ohmmeter (Millipore). Inserts containing pseudo-epithelia were then mounted in an EM-CSYS-6 Ussing chamber system (Physiologic Instruments Inc., USA) composed of two hemi-chambers, each containing a different solution. Asymmetric solutions were used, creating a basal to apical Cl^- gradient to enhance Cl^- currents detection. Their composition was (in mM): 1.2 NaCl, 115 Na-Gluconate, 25 $NaHCO_3$, 1.2 $MgCl_2$, 4 $CaCl_2$, 2.4 KH_2PO_4, 1.24 K_2HPO_4, 10 mannitol (pH 7.4) for apical solution and 115 NaCl, 25 $NaHCO_3$, 1.2 $MgCl_2$, 1.2 $CaCl_2$, 2.4 KH_2PO_4, 1.24 K_2HPO_4, 10 glucose (pH 7.4) for basal solution. Apical and basal solutions were maintained around physiological temperature (35-38°C) and gassed with 95% O_2 - 5% CO_2. Transepithelial potential difference and short-circuit currents were measured/injected through 3M KCl filled Ag/AgCl electrodes connected to a VCC MC2 voltage/current clamp (Physiologic Instruments Inc., USA). Visualization and recording of the current injected by the system to short-circuit pseudo-epithelia (clamp at 0 mV) was visualized and recorded at a frequency of 0.1 Hz on a personal computer using Acquire and Analyze hardware and software (Physiologic Instruments Inc., USA). Transepithelial potential difference values were corrected for the junction potential between apical and basal solutions and for empty insert resistance. Since the polarity of I_{sc} was referred to the basal side of the pseudo-epithelium and a gain of -10 was applied, an apical anion secretion was indicated by an increase in Isc. All experiments were done in the presence of 100 µM amiloride in the apical solution to prevent ENaC currents. All the drugs were added to the apical solution.

4.2.4. Intracellular cAMP measurements

CFBE CFTR-F508del cells were plated in 60 mm diameter culture dishes (400,000 cells per dish). When cells reached 80% confluence, they were treated with test compounds at the concentration leading to the maximal potentiator effect during 15 min at 37°C. Intracellular contents were harvested by incubating cells during 20 min in a 0.1M HCl solution, followed by a centrifugation step at 18000 x g. Intracellular cAMP levels were then measured using a cAMP Direct Immunoassay kit (ab65355, Abcam), according to the kit manufacturer instructions. Data are expressed as the percentage of intracellular cAMP levels detected in solvent treated cells.

4.2.5. Cell viability test:

Hela cells were seeded in 96 well plates (30,000 cells per well). 24h later, cells were incubated at 37°C with test compounds at various concentrations during 24h. Wells were then washed with Phosphate Buffer Saline (PBS) and incubated with a solution of Thiazolyl Blue Tetrazolium Bromide (MTT) (0.5 $mg.mL^{-1}$; Sigma) during 4h before the supernatant was removed. Purple formazan crystals were dissolved in 100 µL dimethylsulfoxide (Sigma) and optical density was measured at 570 nm with a 630 nm correction using a microplate reader (SpectraCount microplate photometer; Packard, Meriden, CT). Data are expressed as the percentage of values obtained for solvent treated cells (DMSO).

4.2.6. Western-blot

Hela cells were lysed (lysis buffer: 10 mM Tris HCl, 1% Nonidet P-40, 0.5% sodium deoxycholate, 1 mM de Pefabloc® SC and protease inhibitors cocktail; pH 7.5). 50 µg of protein were resolved on a 5-10% gradient SDS-PAGE, transferred to a nitrocellulose membrane, immunoblotted using the MAB3480 anti-CFTR antibody and the Na/K ATPase (both mouse monoclonal used at 1:1000; Millipore Corporation, USA), exposed to secondary antibody conjugated to horseradish peroxidase (used at 1:5000; Amersham, GE Healthcare, UK) for 1 hour and revealed by chemiluminescence with ECL Western-blotting reagent (Millipore) and the GeneGnome XRQ chemiluminescence systems (Syngen, Synoptic Ltd, UK).

4.2.7. YFP measurements

After 24 hours, transfected HEK293 cells in 96-well plates were washed with PBS and each well incubated 30 min with 50 µL of PBS containing cpt-cAMP (100µM) and IBMX (100 µM) (all from Sigma-Aldrich) with and without VX-770, SBC040 or SBC219. Plates were then transferred to a ClarioStar plate-reader (BMG) to measure YFP fluorescence. After 3 seconds,

200 µl of PBS-NaI (PBS solution where NaCl is replaced with NaI) were injected. Signal decay was fitted to an exponential function to derive the maximal slope corresponding to initial influx into the cells. Maximal slopes were converted to rates of change in intracellular I^- concentration (in mM/s).

4.2.8. Drugs and chemicals

Amiloride, CFTR(inh)-172, forskolin, genistein, cpt-cAMP and IBMX were purchased from Sigma Aldrich (France). VX-770 and VX-809 were obtained from Selleckchem (USA). Stock solutions of SBCs and other drugs were prepared using dimethyl sulfoxide (DMSO) as solvent.

4.2.9. Data analysis and statistics:

For patch-clamp and Ussing chamber experiments, graphs and statistics were done using Prism 5 (GraphPad Software, USA) and all the results are expressed as mean ± SEM except for box plot representations for which the central line represents the median, boxes upper and lower edges represent the 25^{th} and 75^{th} percentile respectively while the whiskers represent the minimal and maximal values of the sample. Statistical comparisons were made using non-parametric ($n < 10$) or parametric ($n \geq 10$) tests with a significance level of 0.05. Before using a parametric test, samples were checked for normality using Shapiro-Wilk normality test. For Ussing chamber screening data, since these experiments did not require high replication level, a parametric test was used even if the sample size was small and normality of sample distribution could not be tested. For YFP based measurements, quantitative variables are described as mean (± SEM). Comparisons to WT conditions and between treated and untreated conditions were made with one-way ANOVA followed by Fischer test for p evaluation.

4.3. Docking and molecular dynamics simulations

4.3.1. CFTR models

We used the published model of the open form of the CFTR MSD:NBD assembly [25] which was supported by experimental data [44] including recent cryo-electron structures of the full-length CFTR [30]. Based on the wild-type (WT) model, we built using chimera [76, 77] three additional models including mutations. The first corresponds to the most common class II mutant, a CFTR-F508del model while the other models represent class III G551D and G1349D mutants.

4.3.2. Design of SBCs and docking on CFTR

SBC040 and SBC219 were designed using the Ligand Reader & Modeler module of the CHARMM-GUI platform [78-80]t. CHARMM-compatible topology and parameter files were hence generated using the CgenFF tool [81-83]. The ligands were docked either within CFTR canonical or non-canonical sites after a superimposition with the ATP occupying each site. These manual docking was also supported by a docking performed using Autodock Vina [84] and AutoDockTools from MGLTools package with ATP-free CFTR. Using a distance cutoff of 12 Å between the centers of mass of ATP and each SBC position, we found that 45% of positions out of the from the top twenty docking hits were within ATP-binding sites for both SBC040 and SBC219 (by comparison, we found 60 % (SBC040) and 65% (SBC219) matching positions in the cryo-EM hCFTR structure).

4.3.3. Molecular dynamics simulations

Each model was embedded in a lipid bilayer consisting of POPC molecules using the charmm-gui platform [78, 80, 85, 86] and the same protocol as previously described [44] for generating and equilibrating protein-membrane simulations complexes, as well as for the MD simulations (CHARM36 force field [87] with the CMAP correction [88] in NAMD 2.9 [89]). Production phases were conducted (the simulation time of each system is reported in **Figure S7** (supporting information)) at a temperature of 310 K (wild-type CFTR, CFTR-G551D and CFTR-G1349D) or 300 K (for CFTR-F508del) and a pressure of 1 bar.

4.3.4. Contact analysis

The contacts between each SBC and CFTR were analyzed by VLDM (Voronoi Laguerre Delaunay for Macromolecules) [90-92]. VLDM relies on a tessellation method, that is, a partition of space into a collection of polyhedra filling space without overlaps or gaps. The program builds the Delaunay tessellation and its Laguerre dual from a set of atomic data, each atom being characterized by its position in space and a weight depending on its van der Waals radius. For consistency with the simulations, the van der Waals radius values are those of CHARMM36 [87]. In the present analysis, only the heavy atoms of the protein, membrane and solvent were considered. CFTR/SBCs contact maps were realized using R [93].

4.3.5. Cluster analysis

SBCs binding sites were precisely defined by these contact map analyses. Using only these protein sites definition, clustering analyses were performed using the contact map overlap (CMO) as a metric in ClusCo program [94].

4.3.6. Additional Trajectory Analyses

Root Mean Square Deviations (RMSDs) were computed with VMD between the snapshots and the initial configuration derived from CFTR model before the heating and equilibration stages. RMSDs were calculated on protein backbone heavy atoms. Salt bridges and atom pairs distances were calculated using in-house tcl scripts executed in VMD. Figures of RMSDs were prepared using gnu plot 5.0 (http://www.gnuplot.info.).

MD trajectories were visualized with VMD. Snapshots figures were made by CHIMERA [77], Pymol [95] or VMD [96].

4.3.7. Binding Free Energy calculations

We performed Molecular Mechanics/ Generalized Born Surface Area (MMGBSA) calculations using the python script MMPBSA.py (in Ambertools 18) [97] to provide an estimation and a comparison of the binding free energies of the SBCs in their different binding sites. This tool is a post-processing method in which representative snapshots from MD trajectories are used to calculate the free energy change between SBC bound and free state of CFTR. We used default parameters with igb= 2.

ACKNOWLEDGMENTS

This work was performed using HPC resources from GENCI-[CINES] (Grants 2017-A0020707206, 2018-A0040707206, 2019-A006707206) and benefited from the financial support of the French Association Vaincre la Mucoviscidose (VLM) and Association pour l'Aide à la Recherche contre la Mucoviscidose (AARM). It was also partially supported by Labex ARCANE and CBH-EUR-GS (ANR-17-EURE-0003). A.B. was the recipient of post-doctoral fellowship from the CF Trust.

REFERENCES

[1] J.S. Elborn, Cystic fibrosis, Lancet, 388 (2016) 2519-2531.

[2] L. Csanády, P. Vergani, D.C. Gadsby, Structure, gating, and regulation of the CFTR anion channel., Physiol Rev, 99 (2019) 707-738.

[3] G. Veit, R.G. Avramescu, A.N. Chiang, S.A. Houck, Z. Cai, K.W. Peters, J.S. Hong, H.B. Pollard, W.B. Guggino, W.E. Balch, W.R. Skach, G.R. Cutting, R.A. Frizzell, D.N. Sheppard, D.M. Cyr, E.J. Sorscher, J.L. Brodsky, G.L. Lukacs, From CFTR biology toward combinatorial pharmacotherapy: expanded classification of cystic fibrosis mutations., Mol Biol Cell, 27 (2016) 424-433.

[4] F. Van Goor, S. Hadida, P.D. Grootenhuis, B. Burton, J.H. Stack, K.S. Straley, C.J. Decker, M. Miller, J. McCartney, E.R. Olson, J.J. Wine, R.A. Frizzell, M. Ashlock, P.A. Negulescu, Correction of the F508del-CFTR protein processing defect in vitro by the investigational drug VX-809., Proc Natl Acad Sci U S A, 108 (2011) 18843-18848.
[5] C.E. Wainwright, J.S. Elborn, B.W. Ramsey, G. Marigowda, X. Huang, M. Cipolli, C. Colombo, J.C. Davies, K. De Boeck, P.A. Flume, M.W. Konstan, S.A. McColley, K. McCoy, E.F. McKone, A. Munck, F. Ratjen, S.M. Rowe, D. Waltz, M.P. Boyle, T.S. Group, T.S. Group, Lumacaftor-Ivacaftor in Patients with Cystic Fibrosis Homozygous for Phe508del CFTR., N Engl J Med, 373 (2015) 220-231.
[6] D.M. Cholon, N.L. Quinney, M.L. Fulcher , C.R.J. Esther, J. Das, N.V. Dokholyan, S.H. Randell, R.C. Boucher, M. Gentzsch, Potentiator ivacaftor abrogates pharmacological correction of DeltaF508 CFTR in cystic fibrosis. , Sci Transl Med, 6 (2014) 246ra296.
[7] G. Veit, R.G. Avramescu, D. Perdomo, P.W. Phuan, M. Bagdany, P.M. Apaja, F. Borot, D. Szollosi, Y.S. Wu, W.E. Finkbeiner, T. Hegedus, A.S. Verkman, G.L. Lukacs, Some gating potentiators, including VX-770, diminish DeltaF508-CFTR functional expression. , Sci Transl Med, 6 (2014) 246ra297.
[8] P.W. Phuan, G. Veit, J. Tan, A. Roldan, W.E. Finkbeiner, G.L. Lukacs, A.S. Verkman, Synergy-based small-molecule screen using a human lung epithelial cell line yields ΔF508-CFTR correctors that augment VX-809 maximal efficacy., Mol Pharmacol, 86 (2014) 42-51.
[9] C. Boinot, M. Jollivet Souchet , R. Ferru-Clément, F. Becq, Searching for combinations of small-molecule correctors to restore f508del-cystic fibrosis transmembrane conductance regulator function and processing., J Pharmacol Exp Ther, 350 (2014) 624-634.
[10] G. Veit, H. Xu, E. Dreano, R.G. Avramescu, M. Bagdany, L.K. Beitel, A. Roldan, M.A. Hancock , C. Lay, W. Li, K. Morin, S. Gao, P.A. Mak, E. Ainscow, A.P. Orth, P. McNamara, A. Edelman, S. Frenkiel, E. Matouk, I. Sermet-Gaudelus, W.G. Barnes, G.L. Lukacs Structure-guided combination therapy to potently improve the function of mutant CFTRs., Nat Med, 24 (2018) 1732-1742.
[11] G.W. Carlile, Q. Yang, E. Matthes, J. Liao, S. Radinovic, C. Miyamoto, R. Robert, J.W. Hanrahan, D.Y. Thomas, A novel triple combination of pharmacological chaperones improves F508del-CFTR correction., Sci Rep, 8 (2018) 11404.
[12] J. Davies, S.M. Moskowitz, C. Brown, A. Horsley, M.A. Mall, E.F. McKone, B.J. Plant, D. Prais, B.W. Ramsey, J.L. Taylor-Cousar, E. Tullis, A. Uluer, C.M. McKee, S. Robertson, R.A. Shilling, C. Simard, F. Van Goor, D. Waltz, F. Xuan, T. Young, S.M. Rowe, V.-.-S. Group., VX-659-Tezacaftor-Ivacaftor in Patients with Cystic Fibrosis and One or Two Phe508del Alleles., N Engl J Med, 379 (2018) 1599-1611.
[13] D. Keating, G. Marigowda, L. Burr, C. Daines, M.A. Mall, E.F. McKone, B.W. Ramsey, S.M. Rowe, L.A. Sass, E. Tullis, C.M. McKee, S.M. Moskowitz, S. Robertson, J. Savage, C. Simard, F. Van Goor, D. Waltz, F. Xuan, T. Young, J.L. Taylor-Cousar, V.-.-S. Group., VX-445-Tezacaftor-Ivacaftor in Patients with Cystic Fibrosis and One or Two Phe508del Alleles., N Engl J Med, 379 (2018) 1612-1620.
[14] M. Gees, S. Musch, S. Van der Plas, A.S. Wesse, A. Vandevelde, K. Verdonck, O. Mammoliti, T. Hwang, K. Sonck, P. Stouten, A.M. Swensen, M. Jans, J. Van der Schueren, L. Nelles, M. Andrews, K. Conrath, Identification and Characterization of novel CFTR potentiators., Front Pharmacol, 9 (2018) 221.
[15] J. Park , P. Khloya, Y. Seo, S. Kumar, H.K. Lee, D.K. Jeon, S. Jo, P.K. Sharma, W. Namkung, Potentiation of ΔF508- and G551D-CFTR-Mediated Cl- Current by Novel Hydroxypyrazolines., PLoS One, 11 (2016) e0149131.

[16] P.W. Phuan, J.H. Son, J.A. Tan, C. Li, I. Musante, L. Zlock, D.W. Nielson, W.E. Finkbeiner, M.J. Kurth, L.J. Galietta, P.M. Haggie, A.S. Verkman, Combination potentiator ('co-potentiator') therapy for CF caused by CFTR mutants, including N1303K, that are poorly responsive to single potentiators., J Cyst Fibr, 17 (2018) 595-606.
[17] P.W. Phuan, G. Veit, J.A. Tan, W.E. Finkbeiner, G.L. Lukacs, A.S. Verkman, Potentiators of Defective ΔF508-CFTR Gating that Do Not Interfere with Corrector Action., Mol Pharmacol, 88 (2015) 791-799.
[18] L. Byrnes, Y. Xu, X. Qiu, J. Hall, G. West, Sites associated with Kalydeco binding on human Cystic Fibrosis Transmembrane Conductance Regulator revealed by Hydrogen/Deuterium Exchange., Sci Rep, 8 (2018) 4664.
[19] I. Callebaut, B. Hoffmann, J.-P. Mornon, The implications of CFTR structural studies for cystic fibrosis drug development., Curr Opin Pharmacol, 34 (2017) 112-118.
[20] O. Kalid, M. Mense, S. Fischman, A. Shitrit, H. Bihler, E. Ben-Zeev, N. Schutz, N. Pedemonte, P.J. Thomas, R.J. Bridges, D.R. Wetmore, Y. Marantz, H. Senderowitz, Small molecule correctors of F508del-CFTR discovered by structure-based virtual screening., J Comput Aided Mol Des, 24 (2010) 971-991.
[21] S.V. Molinski, V.M. Shahani, A.S. Subramanian, S.S. MacKinnon, G. Woollard, M. Laforet, O. Laselva, L.D. Morayniss, C.E. Bear, A. Windemuth, Comprehensive mapping of cystic fibrosis mutations to CFTR protein identifies mutation clusters and molecular docking predicts corrector binding site., Proteins, 86 (2018) 833-843.
[22] N. Odolczyk, J. Fritsch, C. Norez, N. Servel, M.F. da Cunha, S. Bitam, A. Kupniewska, L. Wiszniewski, J. Colas, K. Tarnowski, D. Tondelier, A. Roldan, E.L. Saussereau, P. Melin-Heschel, G. Wieczorek, G.L. Lukacs, M. Dadlez, G. Faure, H. Herrmann, M. Ollero, F. Becq, P. Zielenkiewicz, A. Edelman, Discovery of novel potent ΔF508-CFTR correctors that target the nucleotide binding domain., EMBO Mol Med, 5 (2013) 1484-1501.
[23] H.-I. Yeh, L. Qiu, Y. Sohma, K. Conrath, X. Zou, T. Hwang, Identifying the molecular target sites for CFTR potentiators GLPG1837 and VX-770., J Gen Physiol, 151 (2019) 912-928.
[24] Z. Zhang, J. Chen, Atomic Structure of the Cystic Fibrosis Transmembrane Conductance Regulator., Cell, 167 (2016) 1586-1597.
[25] J.-P. Mornon, B. Hoffmann, S. Jonic, P. Lehn, I. Callebaut, Full-open and closed CFTR channels, with lateral tunnels from the cytoplasm and an alternative position of the F508 region, as revealed by molecular dynamics., Cell Mol Life Sci, 72 (2015) 1377-1403.
[26] J.-P. Mornon, P. Lehn, I. Callebaut, Atomic model of human cystic fibrosis transmembrane conductance regulator: membrane-spanning domains and coupling interfaces., Cell Mol Life Sci, 65 (2008) 2594-2612.
[27] A.W. Serohijos, T. Hegedus, A.A. Aleksandrov, L. He, L. Cui, N.V. Dokholyan, J.R. Riordan, Phenylalanine-508 mediates a cytoplasmic-membrane domain contact in the CFTR 3D structure crucial to assembly and channel function., Proc Natl Acad Sci U S A, 105 (2008) 3256-3261.
[28] F. Liu, Z. Zhang, L. Csanády, D.C. Gadsby, J. Chen, Molecular structure of the human CFTR ion channel., Cell, 169 (2017) 85-95.
[29] Z. Zhang, F. Liu, J. Chen, Conformational changes of CFTR upon phosphorylation and ATP binding., Cell, 170 (2017) 483-491.
[30] Z. Zhang, F. Liu, J. Chen, Molecular structure of the ATP-bound, phosphorylated human CFTR., Proc Natl Acad Sci U S A, 115 (2018) 12757-12762.
[31] F. Liu, Z. Zhang, A. Levit, J. Levring, K.K. Touhara, B.K. Shoichet, J. Chen, Structural identification of a hotspot on CFTR for potentiation., Science, 364 (2019) 1184-1188.

[32] S. Bach, M. Knockaert, J. Reinhardt, O. Lozach, S. Schmitt, B. Baratte, M. Koken, S. Coburn, L. Tang, T. Jiang, D. Liang, H. Galons, J. Dierick, L. Pinna, F. Meggio, F. Totzke, C. Schachtele, A. Lerman, A. Carnero, Y. Wan, N. Gray, L. Meijer, Roscovitine targets, protein kinases and pyridoxal kinase. , J Biol Chem, 280 (2005) 31208-31219.
[33] M.E. Welsch, S.A. Snyder, B.R. Stockwell, Privileged Scaffolds for Library Design and Drug Discovery Curr. Opin. Chem. Biol, 14 (2010) 347–361.
[34] S. Dinesh, G. Shikha, G. Bhavana, S. Nidhi, S. Dileep, Biological activities of purine analogues and scientific innovation, J Pharm Sci Innov, 1 (2012) 29-34.
[35] P.Y. Lam, C.G. Clark, S. Saubern, J. Adams, M.P. Winters, D.M. Chan, A. Combs, New N- and O-arylations with phenylboronic acids and cupric acetate., Tetrahedron Lett, 39 (1998) 2941–2944.
[36] L.A. Foller, T. Ulven, Direct N9-arylation of purines with aryl halides. , Chem. Commun, 50 (2014) 4997-4999.
[37] M. Dejmek, S. Kovacokova, E. Zbornikova, H. Hrebabecky, M. Sala, M. Dracinsky, R. Nencka, One-pot build-up procedure for the synthesis of variously substituted purine derivatives., RSC Advances, 2 (2012) 6970–6980.
[38] J.-L. Décout, R. Zelli, W. Zeinyeh, B. Boucherle, R. Haudecoeur, Methods for synthesizing diversely substituted purines. PCT Int. Appl. (2018), , in: U.G. Alpes (Ed.), 2018.
[39] R. Zelli, W. Zeinyeh, J.-L. Décout, 6-Chloropurine ribonucleosides from chloropyrimidines: One pot synthesis. , Current Protocols in Nucleic Acid Chemistry, e57 (2018) 1-10.
[40] R. Zelli, W. Zeinyeh, R. Haudecoeur, J. Alliot, B. Boucherle, I. Callebaut, J.-L. Décout, A one-pot synthesis of highly substituted purines., Org. Lett., 19 (2017) 6300–6363.
[41] F. Van Goor, S. Hadida, P.D. Grootenhuis, B. Burton, D. Cao, T. Neuberger, A. Turnbull, A. Singh, J. Joubran, A. Hazlewood, J. Zhou, J. McCartney, V. Arumugam, C. Decker, J. Yang, C. Young, E.R. Olson, J.J. Wine, R.A. Frizzell, M. Ashlock, P. Negulescu, Rescue of CF airway epithelial cell function in vitro by a CFTR potentiator, VX-770., Proc Natl Acad Sci U S A, 106 (2009) 18825-18830.
[42] G. Cui, B.B. Stauffer, B.R. Imhoff, R. A, H.J. S, E.J. Sorscher, N.A. McCarty, VX-770-mediated potentiation of numerous human CFTR disease mutants is influenced by phosphorylation level., Sci Rep, 9 (2019) 13460.
[43] H. Yu, B. Burton, C.J. Huang, J. Worley, D. Cao, J.P.J. Johnson, A. Urrutia, J. Joubran, S. Seepersaud, K. Sussky, B.J. Hoffman, F. Van Goor, Ivacaftor potentiation of multiple CFTR channels with gating mutations., J Cyst Fibros, 11 (2012) 237-245.
[44] B. Hoffmann, A. Elbahnsi, P. Lehn, J.-L. Décout, F. Pietrucci, J.-P. Mornon, I. Callebaut, Combining theoretical and experimental data to decipher CFTR 3D structures and functions., Cell Mol Life Sci 75 (2018) 3829-3855.
[45] A. Billet, J.-P. Mornon, M. Jollivet, P. Lehn, I. Callebaut, F. Becq, CFTR: Effect of ICL2 and ICL4 amino acids in close spatial proximity on the current properties of the channel., J Cyst Fibros, 12 (2013) 737-745.
[46] W. Wang, B.C. Roessler, K.L. Kirk, An electrostatic interaction at the tetrahelix bundle promotes phosphorylation-dependent cystic fibrosis transmembrane conductance regulator (CFTR) channel opening., J Biol Chem, 289 (2014) 30364-30378.
[47] G. Cui, C.S. Freeman, T. Knotts, C.Z. Prince, C. Kuang, N.A. McCarty, Two salts bridges differentially contribute to the maintenance of Cystic Fibrosis Transmebrane Conductance Regulator (CFTR) channel function., J Biol Chem, 288 (2013) 20758-20767.
[48] G. Cui, Z.R. Zhang, A.R. O'Brien, B. Song, N.A. McCarty, Mutation at arginine 352 alters the pore architecture of CFTR., J Membr Biol., 222 (2008) 91-106.

[49] O. Laselva, S. Molinski, V. Casavola, C.E. Bear, Correctors of the Major Cystic Fibrosis Mutant Interact through Membrane-Spanning Domains., Mol Pharmacol, 93 (2018) 612-618.
[50] H.Y. Ren, D.E. Grove, S.A. Houck, P. Sopha, F. van Goor, B.J. Hoffman, D.M. Cyr, VX-809 corrects folding defects in cystic fibrosis transmembrane conductance regulator protein through action on membrane-spanning domain 1., Mol Biol Cell, 24 (2013) 3016-3024.
[51] R.P. Hudson, J.E. Dawson, P.A. Chong, Z. Yang, L. Millen, P.J. Thomas, C.G. Brouillette, J.D. Forman-Kay, Direct binding of the corrector VX-809 to human CFTR NBD1: Evidence of an allosteric coupling between the binding site and the NBD1:CL4 interface., Mol Pharmacol, 92 (2017) 124-135.
[52] W.M. Rabeh, F. Bossard, H. Xu, T. Okiyoneda, M. Bagdany, C.M. Mulvihill, K. Du, S. di Bernardo, Y. Liu, L. Konermann, A. Roldan, G.L. Lukacs, Correction of both NBD1 energetics and domain interface is required to restore ΔF508 CFTR folding and function, Cell, 148 (2012) 150-163.
[53] M. Sigoillot, M. Overtus, M. Grodecka, D. Scholl, A. Garcia-Pino , T. Laeremans, L. He, E. Pardon, E. Hildebrandt, I. Urbatsch, J. Steyaert, J.R. Riordan, C. Govaerts, Domain-interface dynamics of CFTR revealed by stabilizing nanobodies., Nat Commun, 10 (2019) 2636.
[54] L. He, A.A. Aleksandrov, J. An, L. Cui, Z. Yang, C.G. Brouillette, J.R. Riordan, Restoration of NBD1 thermal stability is necessary and sufficient to correct DF508 CFTR folding and assembly., J Mol Biol, 427 (2015) 106-120.
[55] J.D. Hall, H. Wang, L.J. Byrnes, S. Shanker, K. Wang, I.V. Efremov, P.A. Chong, J.D. Forman-Kay, A.E. Aulabaugh, Binding screen for cystic fibrosis transmembrane conductance regulator correctors finds new chemical matter and yields insights into cystic fibrosis therapeutic strategy., Protein Sci, 25 (2016) 360-373.
[56] K.Y. Jih, T.C. Hwang, Nonequilibrium gating of CFTR on an equilibrium theme., Physiology, 27 (2012) 351-361.
[57] S.G. Bompadre, M. Li, T.C. Hwang, Mechanism of G551D-CFTR (cystic fibrosis transmembrane conductance regulator) potentiation by a high affinity ATP analog., J Biol Chem, 283 (2008) 5364-5369.
[58] M.F. Tsai, K.Y. Jih, H. Shimizu, M. Li , T.C. Hwang, Optimization of the degenerated interfacial ATP binding site improves the function of disease-related mutant cystic fibrosis transmembrane conductance regulator (CFTR) channels., J Biol Chem, 285 (2010) 37663-37671.
[59] Z. Zhou, X. Wang, M. Li, Y. Sohma, X. Zou, T.C. Hwang, High affinity ATP/ADP analogues as new tools for studying CFTR gating., J Physiol. , 569 (2005) 447-457.
[60] A.A. Aleksandrov, L. Aleksandrov, J.R. Riordan, Nucleoside triphosphate pentose ring impact on CFTR gating and hydrolysis., FEBS Lett, 518 (2002) 183-188.
[61] Z. Cai, A. Taddei, D.N. Sheppard, Differential sensitivity of the cystic fibrosis (CF)-associated mutants G551D and G1349D to potentiators of the cystic fibrosis transmembrane conductance regulator (CFTR) Cl- channel., J Biol Chem., 281 (2006) 1970-1977.
[62] H. Miki, Z. Zhou, M. Li, T.C. Hwang, S.G. Bompadre, Potentiation of disease-associated cystic fibrosis transmembrane conductance regulator mutants by hydrolyzable ATP analogs., J Biol Chem, 285 (2010) 19967-19975.
[63] P.D. Eckford, C. Li, M. Ramjeesingh, C.E. Bear, Cystic fibrosis transmembrane conductance regulator (CFTR) potentiator VX-770 (ivacaftor) opens the defective channel gate of mutant CFTR in a phosphorylation-dependent but ATP-independent manner., J Biol Chem, 287 (2012) 36639-36649.

[64] K.Y. Jih, T.C. Hwang, Vx-770 potentiates CFTR function by promoting decoupling between the gating cycle and ATP hydrolysis cycle., Proc Natl Acad Sci U S A, 110 (2013) 4404-4409
[65] H. Yeh, Y. Sohma, K. Conrath, T. Hwang, A common mechanism for CFTR potentiators., J Gen Physiol, 149 (2017) 1105-1118.
[66] H.I. Yeh, J.T. Yeh, T.C. Hwang, Modulation of CFTR gating by permeant ions., J Gen Physiol, 145 (2015) 47-60.
[67] W.-Y. Lin, Y. Shoma, T.C. Hwang, Synergistic Potentiation of Cystic Fibrosis Transmembrane Conductance Regulator Gating by Two Chemically Distinct Potentiators, Ivacaftor (VX-770) and 5-Nitro-2-(3-Phenylpropylamino) Benzoate, Mol Pharmac, 90 (2016) 275-286.
[68] W. Wang, G. Li, J.P. Clancy, K.L. Kirk, Activating cystic fibrosis transmembrane conductance regulator channels with pore blocker analogs., J Biol Chem, 280 (2005) 23622-23630.
[69] Caputo, A, A. Hinzpeter, E. Caci, N. Pedemonte, N. Arous, M. Di Duca, O. Zegarra-Moran, P. Fanen, L.J. Galietta, Mutation-specific potency and efficacy of cystic fibrosis transmembrane conductance regulator chloride channel potentiators., J Pharmacol Exp Ther, 330 (2009) 783-791.
[70] P.W. Phuan, J.A. Tan, A.A. Rivera, L. Zlock, D.W. Nielson, W.E. Finkbeiner, P.M. Haggie, A.S. Verkman, Nanomolar-potency 'co-potentiator' therapy for cystic fibrosis caused by a defined subset of minimal function CFTR mutants., Sci Rep, 27 (2019) 17640.
[71] G. Veit, D.F. Da Fonte, R.G. Avramescu, A. Premchandar, M. Bagdany, H. Xu, D. Bensinger, D. Stubba, B. Schmidt, E. Matouk, G.L. Lukacs, Mutation-specific dual potentiators maximize rescue of CFTR gating mutants, J Cyst Fibr, in press (2019).
[72] S.-Y. Huang, D. Bolser, H.-Y. Liu, T.C. Hwang, Molecular modeling of the heterodimer of human CFTR's nucleotide-binding domains using a protein–protein docking approach., J Mol Graph Model, 27 (2009) 822-828.
[73] O. Moran, L.J. Galietta, O. Zegarra-Moran, Binding site of activators of the cystic fibrosis transmembrane conductance regulator in the nucleotide binding domains., Cell Mol Life Sci, 62 (2005) 446-460.
[74] L. Aleksandrov, A. Mengos, X. Chang, A.A. Aleksandrov, J.R. Riordan, Differential interactions of nucleotides at the two nucleotide binding domains of the cystic fibrosis transmembrane conductance regulator., J Biol Chem, 276 (2001) 12918-12923.
[75] A. Billet, L. Froux, J.W. Hanrahan, F. Becq, Development of Automated Patch Clamp Technique to Investigate CFTR Chloride Channel Function., Front Pharmacol, 8 (2017) 195.
[76] T.D. Goddard, C.C. HUang, T.E. Ferrin, Software extensions to UCSF chimera for interactive visualization of large molecular assemblies., Structure, 13 (2005) 473-482.
[77] E.F. Pettersen, T.D. Goddard, C.C. Huang, G.S. Couch, D.M. Greenblatt, E.C. Meng, T.E. Ferrin, UCSF Chimera--a visualization system for exploratory research and analysis., J Comput Chem, 25 (2004) 1605-1612.
[78] S. Jo, T. Kim, V.G. Iyer, W. Im, CHARMM-GUI: A web-based graphical user interface for CHARMM, J Comput Chem, 29 (2008) 1859–1865.
[79] S. Kim, J. Lee, S. Jo, C.L. Brooks, H.S. Lee, W. Im, CHARMM-GUI ligand reader and modeler for CHARMM force field generation of small molecules, J Comput Chem, 38 (2017) 1879-1886.
[80] J. Lee, X. Cheng, J.M. Swails, M.S. Yeom, P.K. Eastman, J.A. Lemkul, S. Wei, J. Buckner, J.C. Jeong, Y. Qi, S. Jo, V.S. Pande, D.A. Case, C.L. Brooks, A.D. MacKerell, J.B. Klauda, W. Im, CHARMM-GUI Input Generator for NAMD, GROMACS, AMBER, OpenMM, and

CHARMM/OpenMM Simulations Using the CHARMM36 Additive Force Field., J Chem Theory Comput, 12 (2016) 405-413.
[81] K. Vanommeslaeghe, E. Hatcher, C. Acharya, S. Kundu, S. Zhong, J. Shim, E. Darian, O. Guvench, P. Lopes, I. Vorobyov, A.D. Mackerell, CHARMM general force field: A force field for drug-like molecules compatible with the CHARMM all-atom additive biological force fields., J Comput Chem, 31 (2010) 671-690.
[82] K. Vanommeslaeghe, A.D. MacKerell, Automation of the CHARMM General Force Field (CGenFF) I: bond perception and atom typing., J Chem Inf Model, 52 (2012) 3144-3154.
[83] K. Vanommeslaeghe, E.P. Raman, A.D. MacKerell, Automation of the CHARMM General Force Field (CGenFF) II: assignment of bonded parameters and partial atomic charges., J Chem Inf Model, 52 (2012) 3155-3168.
[84] O. Trott, A.J. Olson, AutoDock Vina : improving the speed and accuracy of docking with a new scoring function, efficient optimization and multithreading., J Comp Chem 31 (2010) 455-461.
[85] J.B. Klauda, R.M. Venable, J.A. Freites, J.W. O'Connor, D.J. Tobias, C. Mondragon-Ramirez, I. Vorobyov, A.D. MacKerell, R.W. Pastor, Update of the CHARMM all-atom additive force field for lipids: validation on six lipid types., J. Phys. Chem. B, 114 (2010) 7830–7843.
[86] E.L. Wu, X. Cheng, S. Jo, H. Rui, K.C. Song, E.M. Dávila-Contreras, Y. Qi, J. Lee, V. Monje-Galvan, R.M. Venable, J.B. Klauda, W. Im, CHARMM-GUI Membrane Builder toward realistic biological membrane simulations., J Comput Chem, 35 (2014) 1997–2004.
[87] K. Hart, N. Foloppe, C.M. Baker, E.J. Denning, L. Nilsson, A.D. Mackerell, Optimization of the CHARMM additive force field for DNA: Improved treatment of the BI/BII conformational equilibrium, J Chem Theory Comput 8, (2012) 348–362.
[88] A.J. MacKerell, M. Feig, C.I. Brooks, Extending the treatment of backbone energetics in protein force fields: Limitations of gas-phase quantum mechanics in reproducing protein conformational distributions in molecular dynamics simulations. , J Comp Chem 25 (2004) 1400-1415.
[89] J.C. Phillips, R. Braun, W. Wang, J. Gumbart, E. Tajkhorshid, E. Villa, C. Chipot, R.D. Skeel, L. Kalé, K. Schulten, Scalable Molecular Dynamics with NAMD., J Comput Chem, 26 (2005) 1781–1802.
[90] A. Elbahnsi , R. Retureau, M. Baaden, B. Hartmann, C. Oguey, Holding the Nucleosome Together: A Quantitative Description of the DNA-Histone Interface in Solution., J Chem Theory Comput, 14 (2018) 1045-1058.
[91] J. Esque, C. Oguey, A.G. de Brevern, A novel evaluation of residue and protein volumes by means of Laguerre tessellation., J Chem Inf Model, 50 (2010) 947-960.
[92] J. Esque, C. Oguey, A.G. de Brevern, Comparative analysis of threshold and tessellation methods for determining protein contacts., J Chem Inf Model, 51 (2011) 493-507.
[93] T.R. Core, R: A language and environment for statistical computing, in: R.F.f.S. Computing (Ed.), Vienna, Austria, 2015.
[94] M. Jamroz, A. Kolinski, ClusCo: clustering and comparison of protein models. , BMC Bioinformatics, 14 (2013) 62.
[95] W.L. DeLano, PyMOL 0.99, in, 2002.
[96] W. Humphrey, A. Dalke, K. Schulten, VMD - Visual Molecular Dynamics, J Mol Graph, 14 (1996) 33-38.
[97] B.R. Miller, T.D. McGee, J.M. Swails, N. Homeyer, H. Gohlke, A.E. Roitberg, MMPBSA.py: An Efficient Program for End-State Free Energy Calculations., J Chem Theory Comput, 8 (2012) 3314-3321.

Scheme and Figure legends

Figure 1: Chemical structures of SBCs

Scheme 1 : Synthetic schemes of the SBC compounds. Details of the synthesis and NMR spectra are reported in Supplementary Figure S2 A) 4-(2,6-Dichloro-9*H*-purin-9-yl)benzamide (SBC001), B) (9-(4-Carbamoylphenyl)-2-chloro-9*H*-purin-6-yl)-L-serine (SBC005), 4-(6-Amino-2-chloro-9*H*-purin-9-yl)benzamide (SBC040), C) 4-(6-Amino-2-chloro-9*H*-purin-9-yl)benzamide (SBC040), D) (9-(4-Carbamoylphenyl)-2-chloro-9*H*-purin-6-yl)-L-alanine (SBC068), E) 4-(2,6-Diamino-9*H*-purin-9-yl)benzamide (SBC069), F) 4-(6-Amino-9*H*-purin-9-yl)benzamide (SBC071), G) 4-(9*H*-Purin-9-yl)benzamide (SBC183), H) 4-(2-Amino-9*H*-purin-9-yl)benzamide (SBC200), I) 4-(6-Amino-2-((3-phenylpropyl)amino)-9*H*-purin-9-yl)benzamide (SBC219), J) 4-(2-Amino-6-hydroxy-9*H*-purin-9-yl)benzamide (SBC231).

Figure 2: Potentiator effect of SBCs on F508del-CFTR-dependent short-circuit currents in CFBE cells.

A. Representative Ussing chamber traces obtained with a potentiating compound (SBC040, black) and a non-potentiating compound (SBC068, grey) on F508del-CFTR CFBE cells corrected 24 h at 27°C. Compounds were tested at 3 successive concentrations after a pre-exposure to 0.1 µM forskolin (fsk). Fsk (10 µM) + genistein (30 µM) were added before inh172 (10 µM) to determine the maximal effect of a known CFTR potentiator under our conditions. **B.** Grouped data summarizing the results obtained for each SBC tested using the protocol described in A. Results are expressed as the mean cumulative ΔI_{sc} measured after the addition of each molecule, normalized to the ΔI_{sc} obtained with fsk (0.1µM). ns, not significant; *, $p< 0.05$; **, $p< 0.01$; ***, $p< 0.001$; n= 3-5; repeated measures ANOVA and Bonferroni post-tests for each SBC. **C.** Mean dose-response curves obtained with SBC040, SBC219 or VX-770 using Ussing chambers on F508del-CFTR CFBE cells after temperature correction. Data are expressed in percent of the maximal cumulative ΔI_{sc} value obtained for each experiment. n=4-6. **D.** Grouped data of intracellular cAMP measured in F508del-CFTR CFBE cells after a 15-minute treatment with SBC040 (30 µM), SBC219 (10 µM) or fsk (10 µM). Data were normalized to the value obtained with DMSO treatment (represented as a dotted line) for each

experiment and are expressed in percent. Data were tested for statistical difference from 100%. ns, not significant; *, p< 0.05; n= 3-6; Wilcoxon signed rank test.

Figure 3: Potentiator effect of SBCs on F508del-CFTR. Each panel shows the representative traces of test and CFTR(inh)-172 conditions (up) and grouped data (down) of I/V curves obtained in the whole cell patch-clamp configuration (automated patch-clamp) on F508del-CFTR HeLa cells with fsk (1μM) alone (A) or in addition to SBC040 (30 μM) (B), SBC219 (10 μM) (C) or VX-770 (0.1 μM) (D). Mean current values are normalized to cell capacitance and expressed in pA/pF.

Figure 4: Potentiator effect of SBCs on G551D- and G1349D-CFTR (patch clamp experiments). Each panel shows the representative traces (up) and grouped data (down) of I/V curves obtained in the whole cell patch-clamp configuration (manual patch-clamp) on G551D- (A and C) or G1349-CFTR (B and D) HeLa cells. SBC040 (A and B) or SBC219 (C and D) were tested for potentiation on these mutants after CFTR pre-phosphorylation with fsk (10 μM). During each experiment, compounds addition was sequential and when no potentiation was observed, genistein (30 μM) was used to ensure that transfection was efficient. Mean current values are normalized to cell capacitance and expressed in pA/pF.

Figure 5: YFP experiments on class III CFTR mutants. A) Potentiator effect of SBCs. Transport rates for WT and indicated mutant CFTR are measured under basal conditions and in the presence of the CFTR potentiator VX-770 (10 μM), SBC040 (10 and 50 μM) or SBC219 (10 and 50 μM). Are indicated significant differences compared with wild-type control conditions and significant effect of potentiators (p<0.01, ANOVA followed by a Fisher test; **: p<0.01 and *** p< 0.001; #: non-significant). **B) Additive effects of SBCs to VX-770.** Transport rates are measured under basal conditions and in the presence of the CFTR potentiators VX-770 (10 μM), SBC040 (50 μM) or SBC219 (50 μM), alone and in combination. Are indicated significant differences compared with wild-type control conditions and significant effect of potentiators (p< 0.01, ANOVA followed by a Fisher test; **: p< 0.01 and *** p< 0.001; #: non-significant).

Figure 6: Synergy between SBCs and VX-770 effects (Ussing chamber) A. Representative Ussing chamber traces obtained on VX-809-corrected F508del-CFTR CFBE cells using sequential additions of SBC040 (30 μM) and VX-770 (1 μM) or VX-770 and SBC040 after a

pre-activation of CFTR with 0.1 µM of fsk. Amiloride (100 µM) and VX-809 (10 µM) were added to the apical solution at the beginning of each experiment. **B.** Box plots showing the repartition of ΔI_{sc} values measured after test compounds addition, following the protocol described in A. one-way ANOVA and Bonferroni post-tests. **C.** Grouped data showing the repartition of the successive variations of I_{sc} following test compounds additions, according to the protocol presented in A. two-way repeated measures ANOVA and Bonferroni post-tests. **D.** Grouped data showing ΔI_{sc} values measured following the addition of VX-770 (1 µM) either before (left) or after (right) the addition of SBC040 (30 µM). two-tailed Mann-Whitney test. **E.** Grouped data showing ΔI_{sc} values measured following the addition of SBC040 (30 µM) either before (left) or after (right) the addition of VX-770 (1 µM). two-tailed Mann-Whitney test. **F, G, H.** Same as C, D, E using SBC219 (10 µM) instead of SBC040 (30 µM). ns, not significant; *, $p< 0.05$; **, $p< 0.01$; ***, $p< 0.001$.

Figure 7: Topology of the putative SBC040 and SBC219 binding sites

Illustration of representative poses of SBC219 (B) and SBC040 (C), extracted from the most populated cluster (see Material and Methods and **Figure S8**), within their putative binding sites (canonical and non-canonical ATP-binding sites).

Figure 1

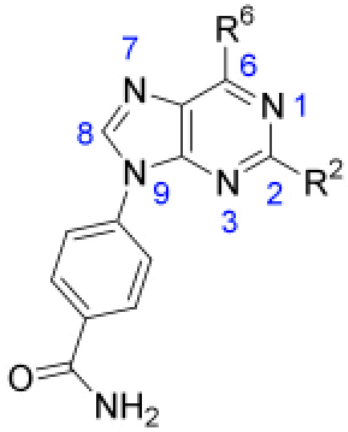

SBC001: $R^2 = R^6 = Cl$

SBC005: $R^2 = Cl$, $R^6 =$ 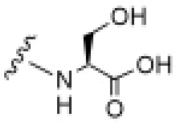

SBC040: $R^2 = Cl$, $R^6 = NH_2$

SBC068: $R^2 = Cl$, $R^6 =$ 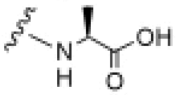

SBC069: $R^2 = R^6 = NH_2$

SBC071: $R^2 = H$, $R^6 = NH_2$

SBC183: $R^2 = R^6 = H$

SBC200: $R^2 = NH_2$, $R^6 = H$

SBC219: $R^2 = NH(CH_2)_3Ph$, $R^6 = NH_2$

SBC231: $R^2 = NH_2$, $R^6 = OH$

Scheme 1

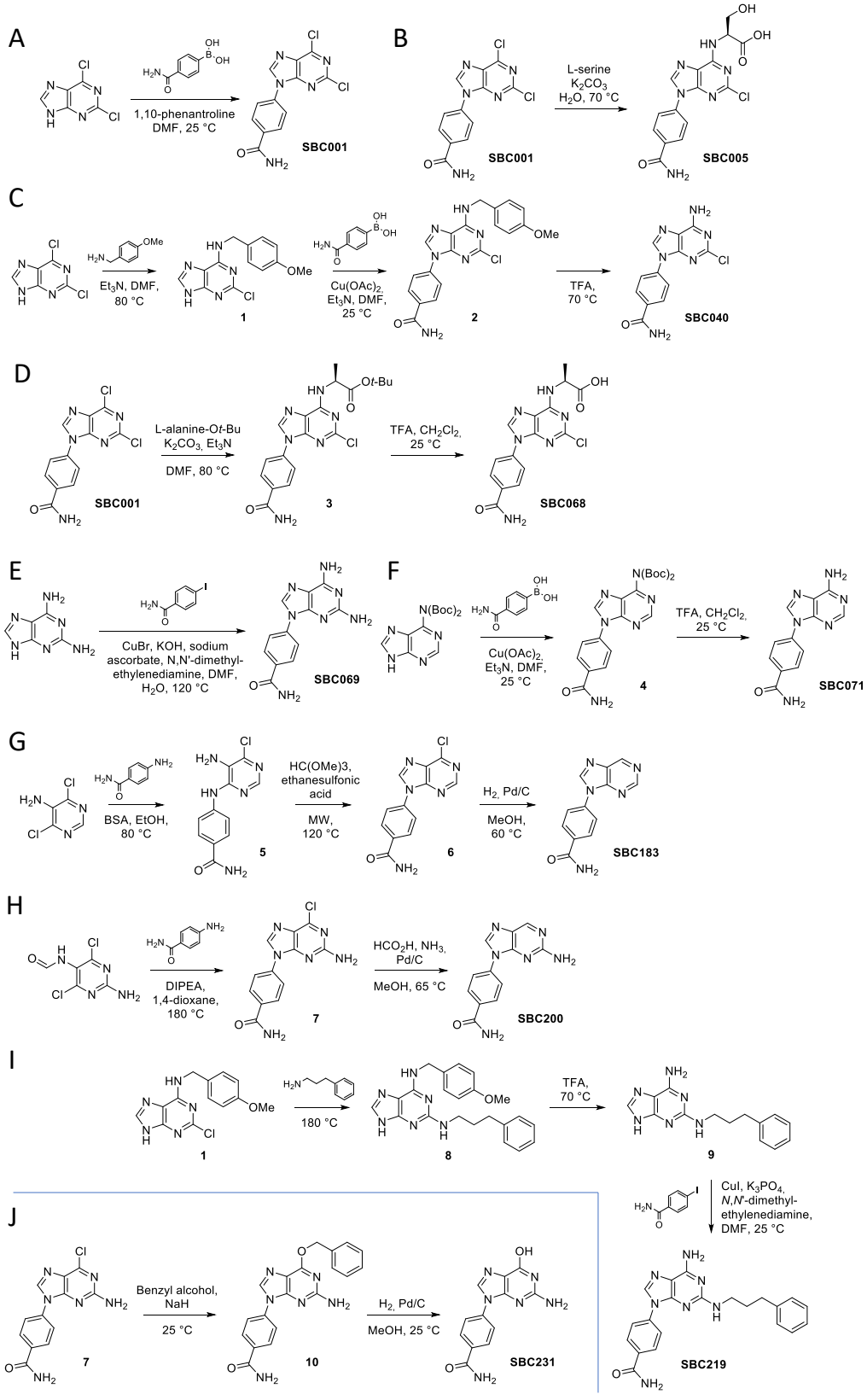
A
1,10-phenantroline
DMF, 25 °C
SBC001
B
L-serine
K2CO3
H2O, 70 °C
SBC001
SBC005
C
Et3N, DMF,
80 °C
1
Cu(OAc)2,
Et3N, DMF,
25 °C
2
TFA,
70 °C
SBC040
D
L-alanine-Ot-Bu
K2CO3, Et3N
DMF, 80 °C
SBC001
3
TFA, CH2Cl2,
25 °C
SBC068
E
CuBr, KOH, sodium
ascorbate, N,N'-dimethyl-
ethylenediamine, DMF,
H2O, 120 °C
SBC069
F
Cu(OAc)2,
Et3N, DMF,
25 °C
4
TFA, CH2Cl2,
25 °C
SBC071
G
BSA, EtOH,
80 °C
5
HC(OMe)3,
ethanesulfonic
acid
MW,
120 °C
6
H2, Pd/C
MeOH,
60 °C
SBC183
H
DIPEA,
1,4-dioxane,
180 °C
7
HCO2H, NH3,
Pd/C
MeOH, 65 °C
SBC200
I
180 °C
1
8
TFA,
70 °C
9
J
Benzyl alcohol,
NaH
25 °C
7
10
H2, Pd/C
MeOH, 25 °C
SBC231
CuI, K3PO4,
N,N'-dimethyl-
ethylenediamine,
DMF, 25 °C
SBC219

Figure 2

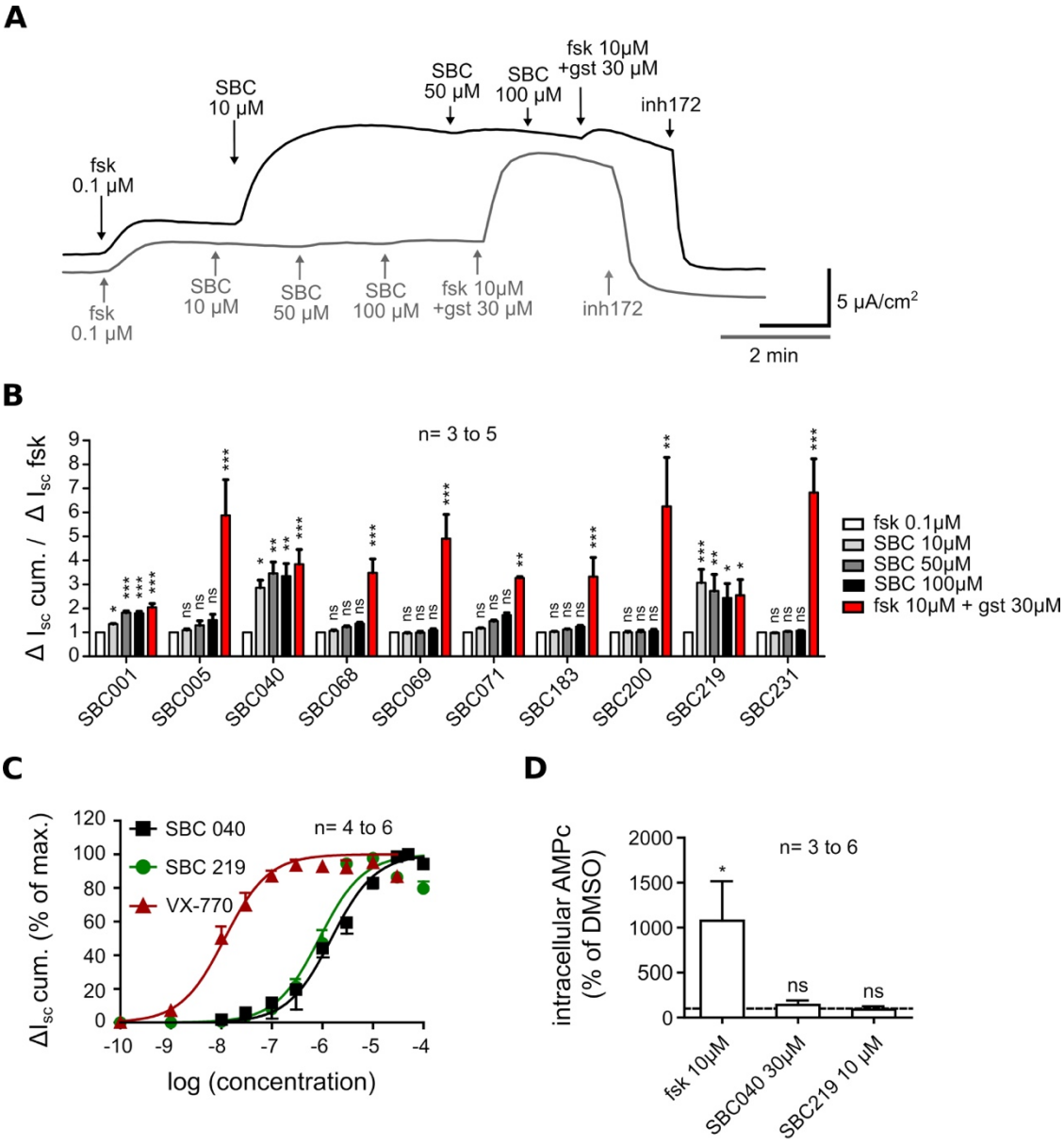
A
fsk 0.1 µM
SBC 10 µM
SBC 50 µM
SBC 100 µM
fsk 10µM +gst 30 µM
inh172
5 µA/cm²
2 min
B
n= 3 to 5
Δ Isc cum. / Δ Isc fsk
fsk 0.1µM
SBC 10µM
SBC 50µM
SBC 100µM
fsk 10µM + gst 30µM
SBC001
SBC005
SBC040
SBC068
SBC069
SBC071
SBC183
SBC200
SBC219
SBC231
C
SBC 040
SBC 219
VX-770
n= 4 to 6
ΔIsc cum. (% of max.)
log (concentration)
D
n= 3 to 6
intracellular AMPc (% of DMSO)
fsk 10µM
SBC040 30µM
SBC219 10 µM

Figure 3

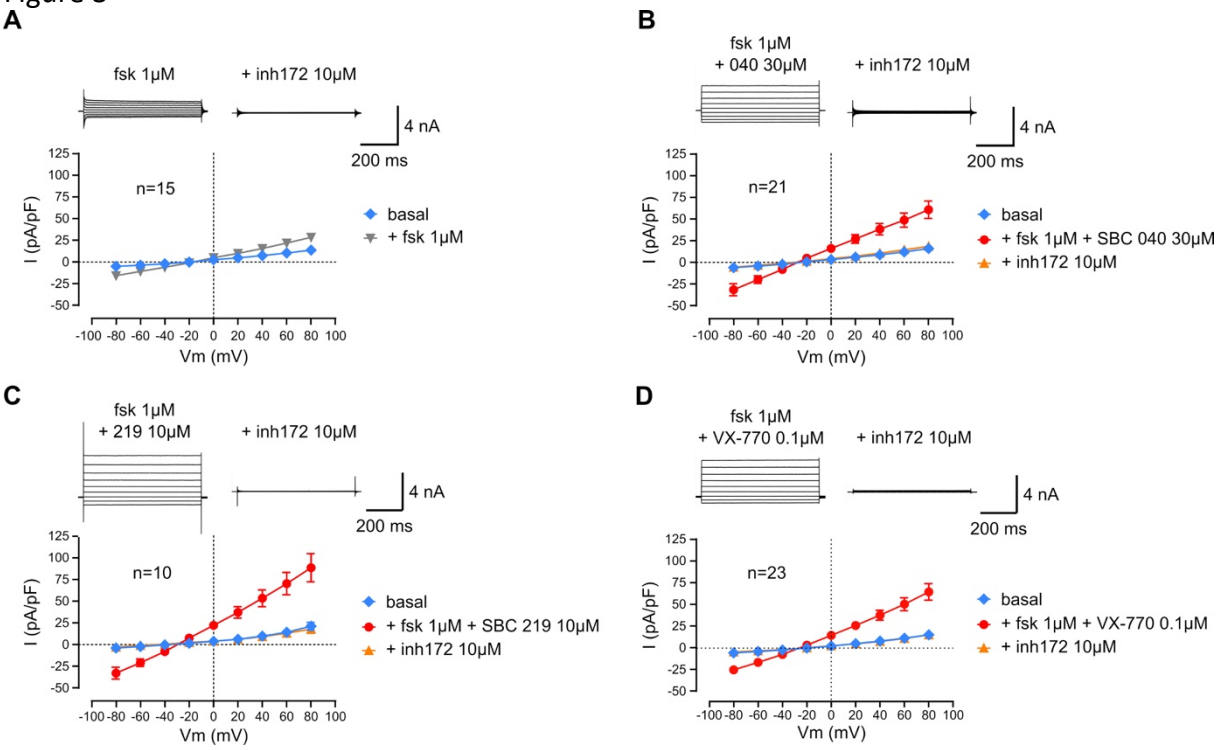
A
fsk 1µM
+ inh172 10µM
4 nA
200 ms
n=15
I (pA/pF)
Vm (mV)
basal
+ fsk 1µM
B
fsk 1µM
+ 040 30µM
+ inh172 10µM
4 nA
200 ms
n=21
I (pA/pF)
Vm (mV)
basal
+ fsk 1µM + SBC 040 30µM
+ inh172 10µM
C
fsk 1µM
+ 219 10µM
+ inh172 10µM
4 nA
200 ms
n=10
I (pA/pF)
Vm (mV)
basal
+ fsk 1µM + SBC 219 10µM
+ inh172 10µM
D
fsk 1µM
+ VX-770 0.1µM
+ inh172 10µM
4 nA
200 ms
n=23
I (pA/pF)
Vm (mV)
basal
+ fsk 1µM + VX-770 0.1µM
+ inh172 10µM

Figure 4

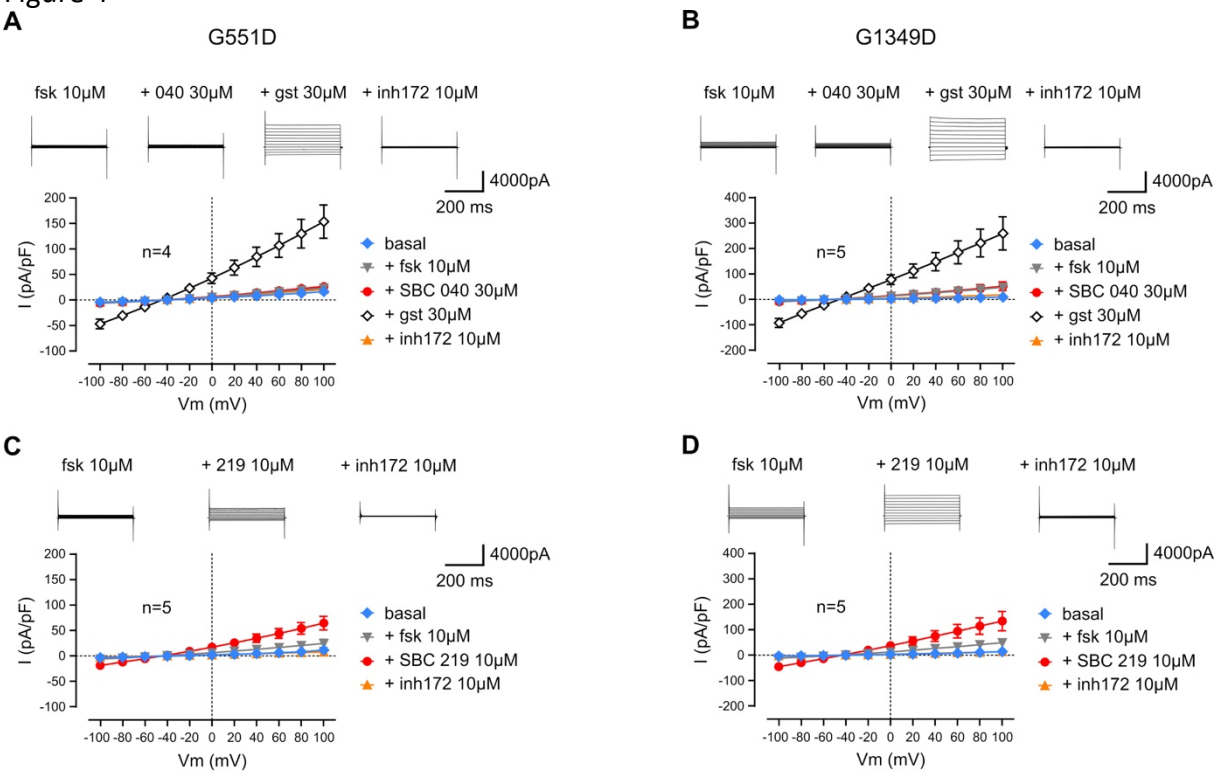
A
G551D
fsk 10µM
+ 040 30µM
+ gst 30µM
+ inh172 10µM
4000pA
200 ms
n=4
I (pA/pF)
Vm (mV)
basal
+ fsk 10µM
+ SBC 040 30µM
+ gst 30µM
+ inh172 10µM
B
G1349D
fsk 10µM
+ 040 30µM
+ gst 30µM
+ inh172 10µM
4000pA
200 ms
n=5
I (pA/pF)
Vm (mV)
basal
+ fsk 10µM
+ SBC 040 30µM
+ gst 30µM
+ inh172 10µM
C
fsk 10µM
+ 219 10µM
+ inh172 10µM
4000pA
200 ms
n=5
I (pA/pF)
Vm (mV)
basal
+ fsk 10µM
+ SBC 219 10µM
+ inh172 10µM
D
fsk 10µM
+ 219 10µM
+ inh172 10µM
4000pA
200 ms
n=5
I (pA/pF)
Vm (mV)
basal
+ fsk 10µM
+ SBC 219 10µM
+ inh172 10µM

Figure 5

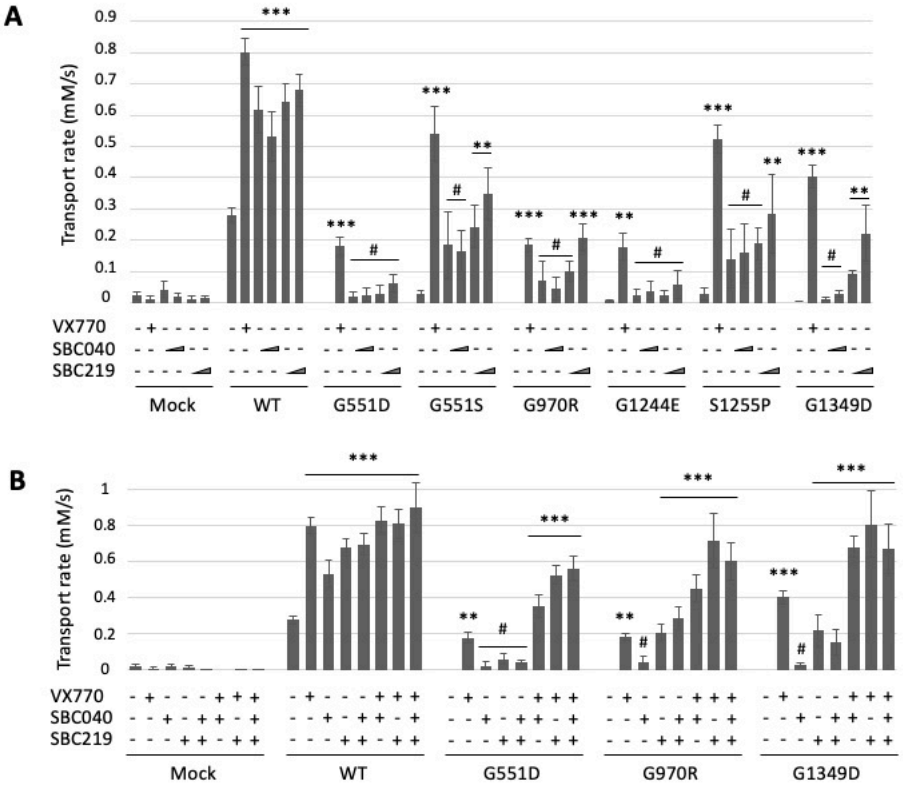
A
Transport rate (mM/s)
0.9
0.8
0.7
0.6
0.5
0.4
0.3
0.2
0.1
0
VX770
SBC040
SBC219
Mock
WT
G551D
G551S
G970R
G1244E
S1255P
G1349D
B
Transport rate (mM/s)
1
0.8
0.6
0.4
0.2
0
VX770
SBC040
SBC219
Mock
WT
G551D
G970R
G1349D

Figure 6

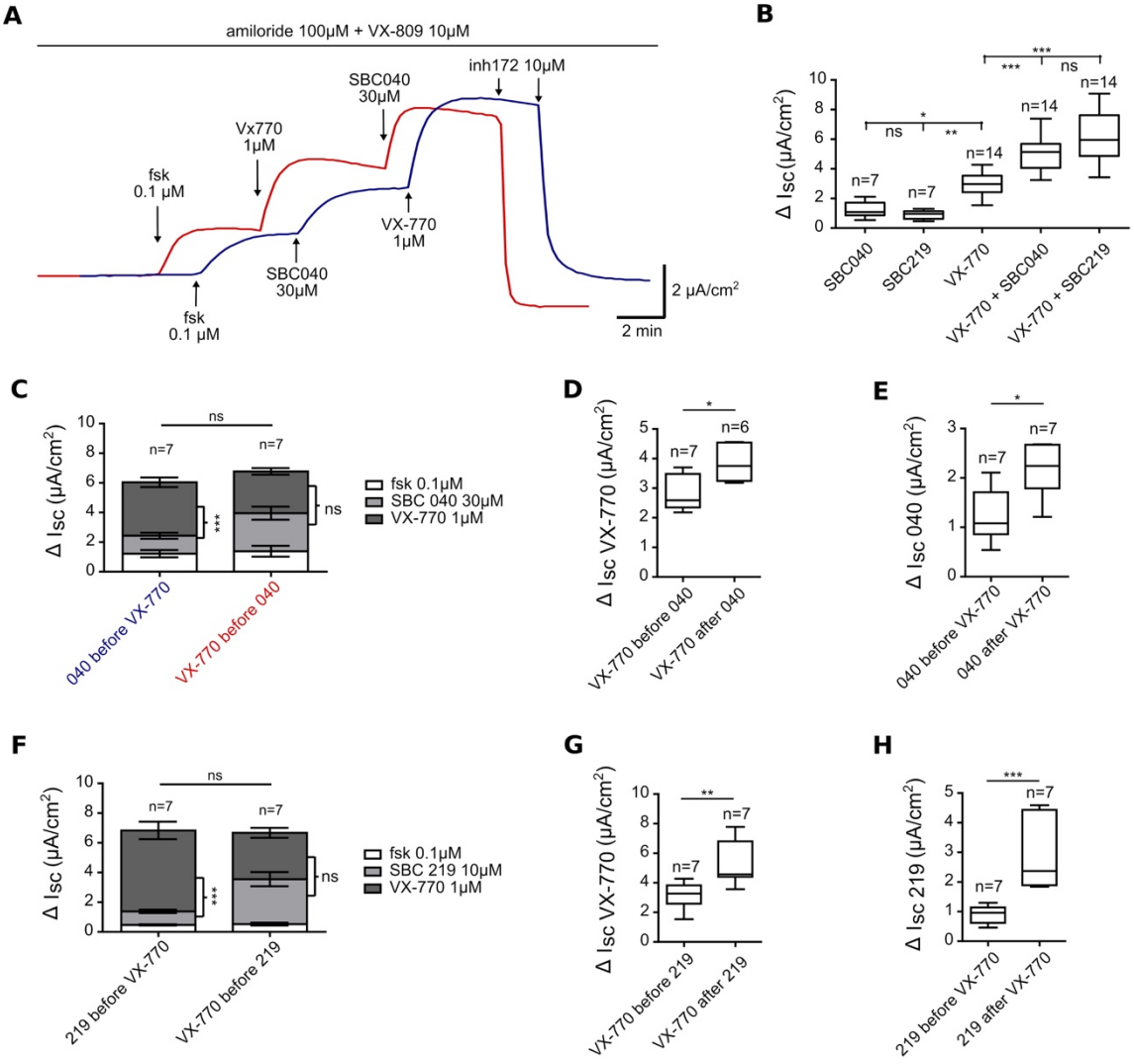
A
amiloride 100µM + VX-809 10µM
inh172 10µM
SBC040 30µM
Vx770 1µM
fsk 0.1 µM
VX-770 1µM
SBC040 30µM
fsk 0.1 µM
2 µA/cm²
2 min
B
Δ Isc (µA/cm²)
n=7
n=7
n=14
n=14
n=14
ns
**
*
***
***
ns
SBC040
SBC219
VX-770
VX-770 + SBC040
VX-770 + SBC219
C
Δ Isc (µA/cm²)
n=7
n=7
ns
***
ns
fsk 0.1µM
SBC 040 30µM
VX-770 1µM
040 before VX-770
VX-770 before 040
D
Δ Isc VX-770 (µA/cm²)
n=7
n=6
*
VX-770 before 040
VX-770 after 040
E
Δ Isc 040 (µA/cm²)
n=7
n=7
*
040 before VX-770
040 after VX-770
F
Δ Isc (µA/cm²)
n=7
n=7
ns
***
ns
fsk 0.1µM
SBC 219 10µM
VX-770 1µM
219 before VX-770
VX-770 before 219
G
Δ Isc VX-770 (µA/cm²)
n=7
n=7
**
VX-770 before 219
VX-770 after 219
H
Δ Isc 219 (µA/cm²)
n=7
n=7
***
219 before VX-770
219 after VX-770

Figure 7

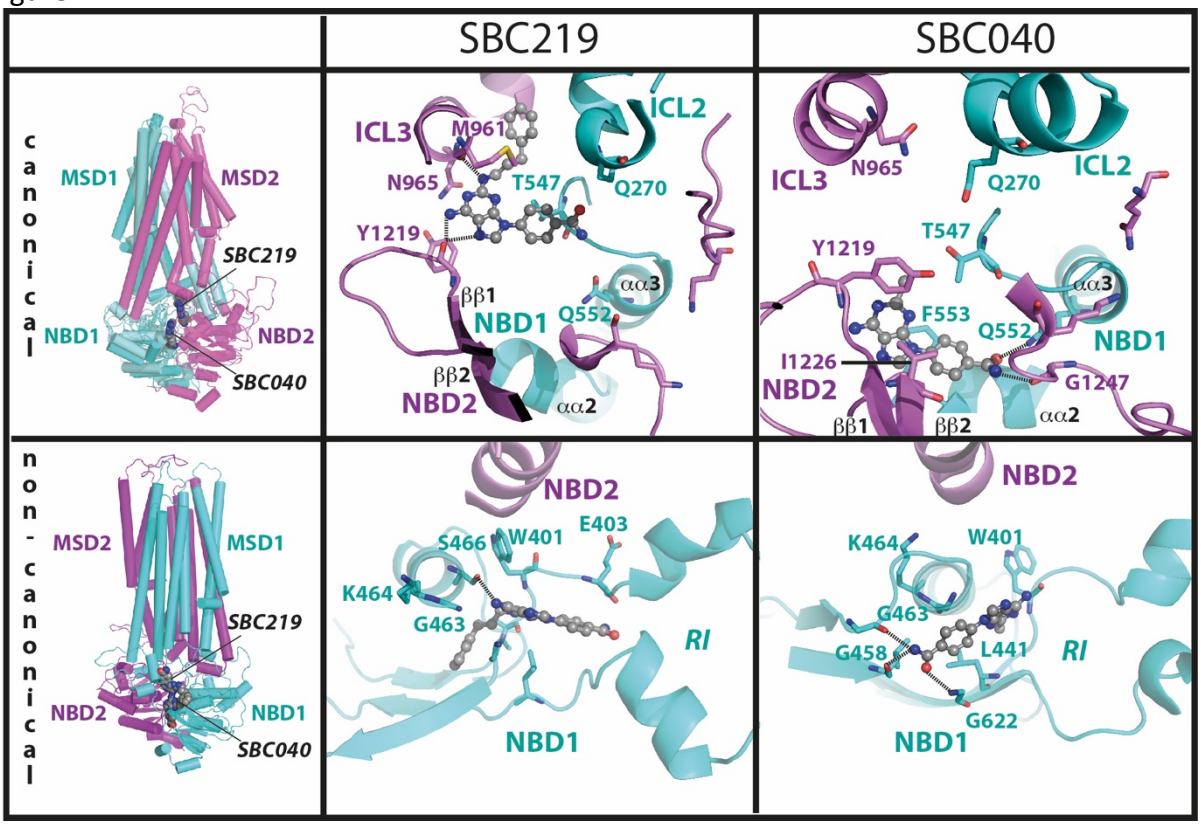
SBC219
SBC040
canonical
non-canonical
MSD1
MSD2
SBC219
NBD1
NBD2
SBC040
ICL3
M961
ICL2
N965
T547
Q270
Y1219
ββ1
NBD1
Q552
αα3
ββ2
NBD2
αα2
F553
I1226
G1247
K464
W401
E403
S466
G463
RI
G458
L441
G622